

Document downloaded from:

<http://hdl.handle.net/10251/66258>

This paper must be cited as:

García-Domene, B.; Sans Tresserras, JÁ.; Manjón Herrera, FJ.; Ovsyannikov, SV.; Dubrovinsky, L.; Martínez-García, D.; Gomis, O.... (2015). Synthesis and High-Pressure Study of Corundum-Type In<sub>2</sub>O<sub>3</sub>. *Journal of Physical Chemistry C*. 119(52):29076-29087. doi:0.1021/acs.jpcc.5b06939.



The final publication is available at

<http://dx.doi.org/10.1021/acs.jpcc.5b06939>

Copyright American Chemical Society

#### Additional Information

This document is the Accepted Manuscript version of a Published Work that appeared in final form in *Journal of Physical Chemistry C*, copyright © American Chemical Society after peer review and technical editing by the publisher. To access the final edited and published work see [insert ACS Articles on Request author-directed link to Published Work, see <http://dx.doi.org/10.1021/acs.jpcc.5b06939>

# Synthesis and High-Pressure Study of Corundum-Type $\text{In}_2\text{O}_3$

*B. García-Domene,<sup>1</sup> J.A. Sans,<sup>2,\*</sup> F. J. Manjón,<sup>2</sup> Sergey V. Ovsyannikov,<sup>3</sup> L.S. Dubrovinsky,<sup>3</sup> D. Martínez-García,<sup>1</sup> O. Gomis,<sup>4</sup> D. Errandonea,<sup>1</sup> H. Moutaabbid,<sup>5</sup> Y. Le Godec,<sup>5</sup> H.M. Ortiz,<sup>2,6</sup> A. Muñoz,<sup>7</sup> P. Rodríguez-Hernández,<sup>7</sup> and C. Popescu<sup>8</sup>*

<sup>1</sup> Departamento de Física Aplicada-ICMUV, MALTA Consolider Team, Universidad de Valencia, Edificio de Investigación, C/Dr. Moliner 50, Burjassot, 46100 Valencia, Spain

<sup>2</sup> Instituto de Diseño para la Fabricación y Producción Automatizada, MALTA Consolider Team-Universitat Politècnica de València, 46022 València, Spain

<sup>3</sup> Bayerisches Geoinstitut, Universität Bayreuth, Universitätsstrasse 30, D-95447, Bayreuth, Germany

<sup>4</sup> Centro de Tecnologías Físicas: Acústica, Materiales y Astrofísica, MALTA Consolider Team, Universitat Politècnica de València, 46022 València, Spain

<sup>5</sup> Institut de Minéralogie, de Physique des Matériaux, et de Cosmochimie (IMPMC)-Sorbonne Universités, UPMC Université Paris 06, UMR CNRS 7590, Muséum National d'Histoire Naturelle, IRD UMR 206, 4 Place Jussieu, F-75005 Paris, France

<sup>6</sup> CINVESTAV-Departamento de Nanociencia y Nanotecnología, Unidad Querétaro, 76230 Querétaro, México

<sup>7</sup> Departamento de Física, Instituto de Materiales y Nanotecnología, MALTA Consolider Team, Universidad de La Laguna, 38205 Tenerife, Spain

<sup>8</sup> CELLS-ALBA Synchrotron, E-08290 Cerdanyola, Barcelona, Spain

KEYWORDS: indium oxide, HP-HT synthesis, corundum, X-ray diffraction, Raman spectroscopy, high-pressure, ab initio calculations

PACS: 61.05.cp, 61.66.Fn, 62.50.-p, 63.20.-e, 71.15.Mb, 78.30.-j

## ABSTRACT

This work reports the high-pressure and high-temperature (HP-HT) synthesis of pure rhombohedral (corundum-type) phase of indium oxide ( $\text{In}_2\text{O}_3$ ) from its most stable polymorph, cubic bixbyite-type  $\text{In}_2\text{O}_3$ , using a multi-anvil press. Structural and vibrational properties of corundum-type  $\text{In}_2\text{O}_3$  (rh- $\text{In}_2\text{O}_3$ ) have been characterized by means of angle-dispersive powder X-ray diffraction and Raman scattering measurements at high pressures which have been compared to structural and lattice dynamics *ab initio* calculations. The equation of state and the pressure dependence of the Raman-active modes of the corundum-type phase are reported and compared to those of corundum ( $\alpha\text{-Al}_2\text{O}_3$ ). It can be concluded that rh- $\text{In}_2\text{O}_3$  is stable under compression up to 15 GPa and it gradually transforms to the orthorhombic  $\text{Rh}_2\text{O}_3$ -III structure between 15 and 26 GPa. The bulk modulus, axial compressibilities and the pressure range of stability of the corundum-type phase in group IIIA sesquioxides  $A_2\text{O}_3$  ( $A=\text{Al}$ , Ga, and In) are discussed.

## INTRODUCTION

The combination of optical transparency and electrical conductivity properties in transparent conducting oxides (TCOs) made them essential in the development of modern optoelectronic devices.<sup>1,2</sup> The most widely studied materials employed for optoelectronic devices that accomplish these properties are several binary oxides like:  $\text{In}_2\text{O}_3$ ,  $\text{Ga}_2\text{O}_3$ ,  $\text{Al}_2\text{O}_3$ , ZnO,  $\text{SnO}_2$  and  $\text{TiO}_2$ .<sup>3-5</sup>

The widespread use of  $\text{In}_2\text{O}_3$  in industrial processes covers the fabrication of window layers in solar cells,<sup>6-8</sup> light-emitting diodes,<sup>9,10</sup> electrochromic windows,<sup>11</sup> liquid-crystal displays,<sup>12,13</sup> and gas sensors.<sup>14,15</sup> Due to the scarcity and high cost to obtain indium metal, new

systems, like Sn-doped  $\text{In}_2\text{O}_3$  (ITO) and corundum-type  $\text{In}_{2-2x}\text{Zn}_x\text{Sn}_x\text{O}_3$  ( $x \leq 0.4$ , or ZITO), have been developed to cut the prize of the production system.<sup>16-18</sup>

At ambient conditions  $\text{In}_2\text{O}_3$  usually crystallizes in the cubic bixbyite-type phase (space group (SG) Ia-3, N. 206, Z=16),<sup>19</sup> and other phases of  $\text{In}_2\text{O}_3$  can be obtained by the application of pressure and temperature: rhombohedral corundum-type (SG R-3c, N. 167, Z=6), orthorhombic  $\text{Rh}_2\text{O}_3$ -II type (SG Pbcn, N. 60, Z= 4), and orthorhombic  $\alpha$ - $\text{Gd}_2\text{S}_3$ -type (SG Pnma, N. 62, Z= 4).<sup>20-41</sup> Moreover, a new orthorhombic  $\text{Rh}_2\text{O}_3$ -III (SG Pbca, N. 61, Z= 8) phase has been recently discovered, which is considered to be the high-pressure structure of corundum-type  $\text{In}_2\text{O}_3$  at ambient temperature.<sup>42</sup> All these phases are going to be named hereafter as c- $\text{In}_2\text{O}_3$ , rh- $\text{In}_2\text{O}_3$ , o1- $\text{In}_2\text{O}_3$ , o2- $\text{In}_2\text{O}_3$  and o3- $\text{In}_2\text{O}_3$ , respectively.

The properties of the high-pressure phases of  $\text{In}_2\text{O}_3$ , some of which can be obtained in a metastable form at ambient conditions, are largely unknown despite their important applications.<sup>37-41</sup> In particular, a decrease on the bulk modulus is expected for the corundum-type structure of sesquioxides  $A_2\text{O}_3$  ( $A= \text{Al}, \text{Ga}, \text{In}$ ) on increasing the cation ionic radius. In fact,  $\text{Cr}^{3+}$ -doped  $\text{Ga}_2\text{O}_3$  was already postulated as a possible substitute of ruby ( $\text{Cr}^{3+}$ -doped  $\text{Al}_2\text{O}_3$ ) for pressure sensor.<sup>43</sup> Similarly, corundum-type  $\text{Cr}^{3+}$ -doped  $\text{In}_2\text{O}_3$  could be more sensitive than ruby as pressure calibrant. With this aim, the knowledge of the equation of state (EOS) and stability range of rh- $\text{In}_2\text{O}_3$  is mandatory. In this respect, the EOS of rh- $\text{In}_2\text{O}_3$  has been studied by means of theoretical calculations,<sup>33,44,45</sup> but the experimental determination of its bulk modulus at ambient pressure has only been estimated by extrapolation of high-pressure data to ambient pressure.<sup>46,47</sup> Furthermore, there is a controversy regarding the pressure range of stability of rh- $\text{In}_2\text{O}_3$ . Gurlo et al. showed that rh- $\text{In}_2\text{O}_3$  is stable at ambient temperature between ambient

pressure and 30 GPa;<sup>37,39</sup> however, in a recent study we have reported that rh-In<sub>2</sub>O<sub>3</sub> undergoes a transformation to o3-In<sub>2</sub>O<sub>3</sub> above 12.4 GPa at 300K.<sup>42</sup>

In this paper, we focus on the structural and vibrational properties of rh-In<sub>2</sub>O<sub>3</sub> under pressure. For that purpose, we have synthesized rh-In<sub>2</sub>O<sub>3</sub> in a multi-anvil cell and characterized it by angle-dispersive powder x-ray diffraction (XRD) and Raman scattering (RS) measurements at high pressure. Experimental structural and vibrational properties of rh-In<sub>2</sub>O<sub>3</sub> have been analysed with the help of theoretical *ab initio* calculations. Our study has allowed us to obtain the bulk modulus of rh-In<sub>2</sub>O<sub>3</sub> at ambient pressure in a more accurate way and shows that the corundum-type phase is only stable up to 15 GPa, because it undergoes a phase transition to the Pbc<sub>a</sub> phase. These results are in good agreement with our previous work.<sup>42</sup> A comparison between the properties of rh-In<sub>2</sub>O<sub>3</sub> and rh-Al<sub>2</sub>O<sub>3</sub> (known as corundum or  $\alpha$ -Al<sub>2</sub>O<sub>3</sub>) at different pressures is discussed and extended to other sesquioxides.

## EXPERIMENTAL DETAILS

Pure rh-In<sub>2</sub>O<sub>3</sub> was synthesized from commercial c-In<sub>2</sub>O<sub>3</sub> (99.99% pure from Sigma-Aldrich Inc.) as starting material using a Sumitomo 1200 tons multi-anvil press to generate high-pressure and high temperature conditions. c-In<sub>2</sub>O<sub>3</sub> was compacted and placed inside a 25  $\mu$ m thickness Re capsule. This metallic capsule was located in a high resistivity graphite furnace, using a MgO cylinder as a spacer. The MgO cylinder isolates electrically the metal capsule from the heater and serves together with graphite as pressure-transmitting medium (PTM). The sample assembly is loaded into a 18 mm MgO:Cr octahedra which is compressed between eight tungsten carbide anvils in the 18/11 multi-anvils configuration. c-In<sub>2</sub>O<sub>3</sub> was maintained for 6 hours at HP-HT conditions (12 GPa and 1375 °C). Subsequently, the sample was quenched in temperature

and decreased slowly in pressure. The recovered sample was composed of different micron sized crystals of rh-In<sub>2</sub>O<sub>3</sub>. These crystals were annealed to 300 °C during 3 hours in a furnace to improve the crystallinity of the sample and ground to obtain fine rh-In<sub>2</sub>O<sub>3</sub> powder.

Room-temperature angle-dispersive powder XRD and RS experiments at high pressures were conducted in annealed rh-In<sub>2</sub>O<sub>3</sub> samples up to 15.9 and 30.0 GPa, respectively, in a membrane-type diamond anvil cell (DAC). In both experiments, powder sample was loaded inside a 150 μm diameter hole drilled in an inconel gasket together with a mixture of methanol-ethanol-water in a 16:3:1 proportion as a PTM. For pressure calibration in angle-dispersive powder XRD and RS measurements we introduced inside the pressure cavity Cu powder<sup>48</sup> and ruby,<sup>49</sup> respectively. Our measurements in rh-In<sub>2</sub>O<sub>3</sub> allow direct comparison with previous experiments in isostructural compounds; e.g., rh-Al<sub>2</sub>O<sub>3</sub>, studied with different PTM.

On the one hand, angle-dispersive powder XRD measurements at different pressures were performed in the MSPD beamline<sup>50</sup> at ALBA synchrotron facility. This beamline is equipped with Kirkpatrick-Baez mirrors to focus the monochromatic beam and a Rayonix CCD detector with a sensitive area of 165 mm. We used a wavelength of 0.4246 Å and the sample-detector distance during the experiment was set to 244.0347 mm (refined value). The 2-D diffraction images were integrated with FIT2D software.<sup>51</sup> Lattice parameters of XRD patterns were obtained with Rietveld refinements performed using POWDERCELL<sup>52</sup> and GSAS<sup>53</sup> program packages. On the other hand, RS measurements at ambient temperature and different pressures were excited using the 632.8 nm HeNe laser and collected in backscattering geometry with a Horiba Jobin Yvon LabRam HR UV spectrometer equipped with a thermoelectrically cooled multichannel CCD detector (resolution below 2 cm<sup>-1</sup>). RS spectra have been analyzed by

fitting Raman peaks with a Voigt profile by fixing the Gaussian linewidth to the experimental setup resolution in order to obtain the three free parameters of the Lorentzian profile.

## THEORETICAL CALCULATIONS

Total-energy *ab initio* calculations were performed for both rh-In<sub>2</sub>O<sub>3</sub> and  $\alpha$ -Al<sub>2</sub>O<sub>3</sub> within the density functional theory (DFT)<sup>54</sup> using the Vienna *Ab initio* Simulation Package (VASP).<sup>55</sup> In particular, we have used the projector-augmented wave (PAW)<sup>56</sup> scheme implemented in this package. The PAW method takes into account the full nodal character of the all-electron charge density distribution in the core region. The generalized gradient approximation (GGA) was used for the description of the exchange-correlation energy with the PBEsol prescription.<sup>57</sup> The set of plane waves employed extended up to a kinetic energy cutoff of 520 eV due to the presence of oxygen and we used dense special k-point grids appropriate to sample the Brillouin zone (BZ). The cutoff energy and the k-point sampling employed ensure a high convergence of 1-2 meV per formula unit in the total energy as well as an accurate calculation of the forces on the atoms. At each selected volume, the structure was fully relaxed to their optimized configuration through the calculation of the forces on atoms and the stress tensor.<sup>57</sup> For each relaxed configuration, the forces on the atoms were smaller than 0.005 eV/Å, and the deviations of the stress tensor from a diagonal hydrostatic form were less than 0.1 GPa. We obtain a set of E, V, and P (pressure, like others energy derivatives, is obtained theoretically from the value of the calculated stress tensor) for each phase as well as the evolution of its structural properties with increasing pressure.

We have also performed lattice dynamics calculations of the phonon modes in rh-In<sub>2</sub>O<sub>3</sub> at the center of the BZ ( $\Gamma$  point). Our theoretical results enable us to assign the Raman-active modes observed in corundum-type In<sub>2</sub>O<sub>3</sub> (see **Fig. 1b**) because calculations provide information

about the symmetry of the modes and polarization vectors, which is not readily accessible in the present experiment. Highly converged results on forces are required for the calculation of the dynamical matrix. We used the direct force constant approach (or supercell method).<sup>58</sup> The construction of the dynamical matrix at the  $\Gamma$  point of the BZ involves separate calculations of the forces in which a fixed displacement from the equilibrium configuration of the atoms within the cell is considered. The use of crystal symmetries aids by reducing the number of such independent displacements, and consequently the computational effort required to study of the different structures considered in this work. Diagonalization of the dynamical matrix provides both the frequencies of the normal modes and their polarization vectors. This theoretical procedure was also used to explain satisfactorily the pressure dependence of the structural and vibrational properties in *c*-In<sub>2</sub>O<sub>3</sub> up to 30 GPa with similar experimental conditions as those in this work.<sup>59</sup>

## RESULTS AND DISCUSSION

### A) Characterization of samples at ambient conditions

**Figure 1** shows angle-dispersive powder XRD pattern **(a)** and RS spectra **(b)** at ambient pressure of both as-grown and annealed samples of In<sub>2</sub>O<sub>3</sub>. A typical CCD images of X-ray diffraction is showed in **Figure S1** in the supplementary material. The powder XRD pattern of the annealed sample has been indexed with DICVOL06<sup>60</sup> obtaining lattice parameters  $a = 5.4854$  Å and  $c = 14.5107$  Å in an hexagonal crystal system with figures of merit  $M(17) = 27.2$  and  $F(17) = 75.2$ . The observed systematic extinctions correspond with the R-3c space group of the corundum-type structure. Rietveld refinement of experimental angle-dispersive powder XRD pattern of the annealed sample at ambient conditions yields experimental lattice parameters and

atomic positions which compare well to those from our *ab initio* theoretical calculations (see **Table I**) and also with previous experiments and calculations.

The corundum-type structure has a primitive unit cell with 2 formula units. Group theory predicts that this structure should have 30 vibrational modes with the irreducible representation<sup>61</sup>

$$\Gamma_{30} = 2A_{1g}(R) + 2A_{2u}(IR) + 5E_g(R) + 4E_u(IR) + 2A_{1u} + 3A_{2g} + A_{2u} + E_u$$

where  $E$  modes are doubly degenerated. These vibrational modes can be divided into 3 acoustic modes ( $A_{2u}$  and  $E_u$ ) and 27 optical modes, thus resulting in 7 Raman-active (R) modes, 6 infrared-active (IR) modes, and 5 silent ( $A_{1u}$  and  $A_{2g}$ ) modes. In fact, **Fig. 1(b)** shows seven Raman-active modes in our samples. The Raman spectrum is dominated by the lowest-frequency  $A_{1g}$  mode located at  $161 \text{ cm}^{-1}$  at ambient pressure. The number of Raman-active modes and the frequencies and intensities are in good agreement with previous studies reporting the synthesis of rh- $\text{In}_2\text{O}_3$ .<sup>25,35</sup> Therefore, our RS measurements confirm the corundum-type structure of our samples. Three broad extra Raman-modes, denoted with asterisks in **Fig. 1(b)**, are observed in as-grown samples but disappear after the annealing process. These extra modes, whose origin is unknown but which do not correspond to other known polymorphs of  $\text{In}_2\text{O}_3$ , could be second-order modes which are better observed in slightly defective samples with small grains and low-crystalline quality than in annealed samples with larger grains and better crystalline quality.

## B) XRD measurements at high pressures

**Figure 2(a)** displays a selection of the experimental angle-dispersive powder XRD patterns of rh- $\text{In}_2\text{O}_3$  at ambient temperature at different pressures up to 15.9 GPa. Bragg reflections located at  $\sim 11.7$  and  $13.5$  degrees at 1.2 GPa correspond to (111) and (200) cubic (Fm-3m) Cu, respectively and were used to determine the pressure inside the DAC. The rest of the Bragg reflections at 1.2 GPa can be attributed to rh- $\text{In}_2\text{O}_3$ . Above 5 GPa, hexagonal

( $P6_3/mmc$ ) Re Bragg reflections (see # marks) appear in the XRD pattern. Probably, a small flake of Re metallic layer, which protects the sample from possible contaminations during the synthesis process, has been unintentionally mixed with the powdered sample. Note that Rietveld refinement was performed using the complete XRD patterns in order to keep as much information as possible from our experimental data. In the experiment, the pressure was smoothly increased up to 15.9 GPa and then released down to 1 GPa (see XRD pattern of the recovered sample in **Fig. 2(a)**). Diffractograms up to 13.5 GPa can be indexed with rh-In<sub>2</sub>O<sub>3</sub>. At 14.5 GPa, the beginning of the phase transition from rh-In<sub>2</sub>O<sub>3</sub> to o3-In<sub>2</sub>O<sub>3</sub> is observed. Both structures coexist until the maximum pressure reached in the XRD experiment (see Rietveld refinements in **Fig. 2(b)**). **Tables S1, S2 and S3** (in the supplementary material) summarize the experimental lattice parameters and atomic positions obtained from Rietveld refinements shown in the **Fig 2(b)** and their comparison with theoretical calculations at similar pressures. The results for both rh-In<sub>2</sub>O<sub>3</sub> and o3-In<sub>2</sub>O<sub>3</sub> are in good agreement with our previous results.<sup>42</sup> Consequently, the larger stability of the corundum-type phase previously reported by Gurlo *et al.* could be related to the nanocrystalline size of the samples synthesized by those authors, which were obtained by compressing nanocrystalline c-In<sub>2</sub>O<sub>3</sub>.<sup>37</sup> Finally, we want to comment that rh-In<sub>2</sub>O<sub>3</sub> is recovered on decreasing pressure, thus showing the reversibility of the rh-In<sub>2</sub>O<sub>3</sub> to o3-In<sub>2</sub>O<sub>3</sub> transition in good agreement with our previous work.<sup>42</sup>

We must note that Bragg reflections in our experiment show a slight broadening with increasing pressure above 10 GPa which could be due to a slight loss of quasi-hydrostatic conditions of the PTM.<sup>62</sup> In this respect, small non-hydrostatic stresses should not influence the structural stability of relatively incompressible ( $B_0 > 150$  GPa) compounds as sesquioxides.<sup>63</sup>

We will show below that this hypothesis is well supported by the good agreement between experiments and theoretical calculations.

**Figure 3** graphs the experimental and theoretical pressure dependence of the unit cell volume of rh-In<sub>2</sub>O<sub>3</sub>. Both experimental and theoretical data were fitted to a third-order Birch-Murnaghan EOS<sup>64,65</sup> in the hydrostatic region of the PTM (below 11 GPa). Again, a rather good agreement between the experimental and theoretical EOS is found. Taking into account the unit cell volume of rh-In<sub>2</sub>O<sub>3</sub> at ambient pressure ( $V_0 = 62.86$  (3) Å<sup>3</sup>), we have estimated the density ( $\rho_{\text{rh}} = 7.398$  (4) g/cm<sup>3</sup>) of rh-In<sub>2</sub>O<sub>3</sub> at ambient pressure in good agreement with previous estimations.<sup>21,22</sup> These values can be compared to the values reported in the literature for volume ( $V_0 = 64.28$  Å<sup>3</sup>) and density ( $\rho_c = 7.179$  g/cm<sup>3</sup>) of c-In<sub>2</sub>O<sub>3</sub> at ambient pressure.<sup>42</sup>

Our experimental bulk modulus at ambient pressure for rh-In<sub>2</sub>O<sub>3</sub> ( $B_0 = 176$  (7) GPa) matches in between our theoretical GGA-PBESol calculations (158 GPa) and previous calculations (176-184 GPa) using local density approximation (LDA).<sup>33,44,45</sup> Clearly, our experimental bulk modulus for rh-In<sub>2</sub>O<sub>3</sub> is consistent with theoretical values and considerably smaller than previous experimental values (212-215 GPa),<sup>46,47</sup> which were obtained from XRD measurements performed only in the high-pressure region.

**Table II** summarizes our experimental and theoretical results for the equation of state of rh-In<sub>2</sub>O<sub>3</sub> along with results from the literature for several sesquioxides in different phases. It is rather curious that the bulk modulus of rh-In<sub>2</sub>O<sub>3</sub> is smaller than that of c-In<sub>2</sub>O<sub>3</sub> despite the smaller volume of the rhombohedral corundum-type phase compared to the cubic phase. In fact, a volume (density) decrease (increase) of around 3.0% is found when the crystal structure going from c-In<sub>2</sub>O<sub>3</sub> to rh-In<sub>2</sub>O<sub>3</sub>. Both the smaller experimental volume and bulk modulus of rh-In<sub>2</sub>O<sub>3</sub> compared to c-In<sub>2</sub>O<sub>3</sub> are in good agreement with our *ab initio* calculations which show similar

trends (see **Table II**). In contrast, a much smaller bulk modulus has been found in rh-In<sub>2</sub>O<sub>3</sub> (176 GPa) than in the corundum-type phases of Al<sub>2</sub>O<sub>3</sub> and Ga<sub>2</sub>O<sub>3</sub>, whose bulk moduli are well above 220 GPa (see **Table II**).<sup>33,66,67</sup> This trend is in good agreement with the larger volume of the corundum-type phase in In<sub>2</sub>O<sub>3</sub> than in Ga<sub>2</sub>O<sub>3</sub> and Al<sub>2</sub>O<sub>3</sub> and is also in good agreement with available theoretical calculations (especially with our own calculations in both In<sub>2</sub>O<sub>3</sub> and Al<sub>2</sub>O<sub>3</sub> using GGA-PBESol for the sake of comparison). Thus, the agreement of experimental and theoretical results supports the goodness of our calculations. It is also noteworthy that the bulk modulus of rh-In<sub>2</sub>O<sub>3</sub> is much smaller than the bulk modulus of corundum-type Ti<sub>2</sub>O<sub>3</sub> (>206 GPa),<sup>68,69</sup> and Cr<sub>2</sub>O<sub>3</sub> (222-231 GPa)<sup>70,71</sup> taking fixed  $B_0' = 4$ . A comparison with corundum-type Fe<sub>2</sub>O<sub>3</sub> and V<sub>2</sub>O<sub>3</sub> is not possible since these two sesquioxides show controversial results with bulk moduli ranging from 150 GPa to 260 GPa.<sup>70,72-76</sup> Our theoretical estimations for both compounds are of the order or larger than 200 GPa and at present we have no idea for the possible deviation between experimental and calculated bulk moduli in these two compounds. In summary, our structural results confirm that rh-In<sub>2</sub>O<sub>3</sub> is one of the sesquioxides with corundum-type structure with the smallest bulk modulus.

**Figure 4** shows the experimental and theoretical pressure dependence of the  $a$  and  $c$  lattice parameters in rh-In<sub>2</sub>O<sub>3</sub> in the hydrostatic region of the PTM. For comparison, we have included in **Fig. 4** the lattice parameters obtained in the downstroke and those obtained at ambient pressure in crystals of rh-In<sub>2</sub>O<sub>3</sub> by Bekheet et al.<sup>41</sup> Both  $a$  and  $c$  parameters have been fitted to a modified Murnaghan's equation of state with free parameters  $a_0$ ,  $B_0$  and  $B_0'$ .

$$a = a_0 \left( 1 + \frac{B_0'}{B_0} P \right)^{-\left( \frac{1}{3B_0'} \right)}, \quad \text{Eq. (1)}$$

The results of these fits are shown in **Table III**. The axial compressibilities of the  $a$ - and  $c$ -axis defined as  $\kappa_x = \frac{-1}{x} \frac{\partial x}{\partial P}$  ( $x = a, c$ ) can be obtained as  $\kappa_x = \frac{1}{3B_0}$  with the  $B_0$  values obtained from the fit of the lattice parameters to Eq. (1). It can be observed that the  $c$  lattice parameter is more compressible than the  $a$  lattice parameter. There is a much better agreement between the experimental and theoretical evolution of the  $a$  lattice parameter than of  $c$  lattice parameter with pressure, despite both experimental and theoretical data show similar trends. Furthermore, one can compare the relative compressibilities of the experimental lattice parameters of isostructural rh-In<sub>2</sub>O<sub>3</sub> and rh-Al<sub>2</sub>O<sub>3</sub>.<sup>77</sup> The experimental relative compressibility of the  $a$  ( $c$ ) lattice parameter defined by  $\Delta a/a_0$  ( $\Delta c/c_0$ ) is 1.57% (3.69%) for rh-In<sub>2</sub>O<sub>3</sub> and 0.96% (1.34%) for rh-Al<sub>2</sub>O<sub>3</sub> in the same pressure range (up to 15.9 GPa).<sup>49,66,70,78-80</sup> Consequently, we can conclude that the major contribution to the increase of sensitivity of the crystalline structure of rh-In<sub>2</sub>O<sub>3</sub> to pressure compared to rh-Al<sub>2</sub>O<sub>3</sub> comes from the larger compressibility along the  $c$  axis in rh-In<sub>2</sub>O<sub>3</sub> than in rh-Al<sub>2</sub>O<sub>3</sub>.

In order to understand the larger compressibility of rh-In<sub>2</sub>O<sub>3</sub> compared to rh-Al<sub>2</sub>O<sub>3</sub> we have studied the evolution under pressure of the theoretically calculated cation-anion distances in both compounds (see **Fig. 5**). Unlike the cubic bixbyite-type structure of  $A_2O_3$  sesquioxides, which has two non-equivalent  $A$  atoms surrounded by six O atoms, the corundum-type structure is characterized by only one type of  $A$  atoms (12c Wyckoff position). The  $A$  atom is surrounded by six O atoms (18e Wyckoff position) forming an octahedron composed of two connected trigonal pyramids (see inset of **Fig. 5**). This structure is then structurally characterized by  $a$  and  $c$  lattice parameters and two internal parameters: the  $z$  internal parameter (off-center position in the octahedra) of the  $A$  atom and the  $x$  atomic coordinate of the O atom. In the most regular atom distribution of the corundum-type structure,  $A$  atoms are located at  $(0, 0, 1/6)$ , while O atoms are

located at  $(1/3, 0, 1/4)$ . Therefore, our experimental and theoretical data at ambient pressure (see **Table I**) indicate that rh-In<sub>2</sub>O<sub>3</sub> has a slightly distorted corundum-type structure. **Figure S2** shows the theoretical and experimental atomic positions ( $x$  of O and  $z$  of In) obtained from Rietveld refinements up to 5 GPa. Moreover, the pressure dependence (quadratic fit) of the theoretical atomic positions of O and In in rh-In<sub>2</sub>O<sub>3</sub> is shown in **Table S4**. The good agreement between experimental and theoretical data observed in **Fig. S2** gives confidence to use our calculated data at higher pressures in order to discuss the pressure dependence of cation-anion bond distances.

The octahedral volume of rh-In<sub>2</sub>O<sub>3</sub> at ambient pressure (13.47 Å<sup>3</sup>) is larger than that of rh-Al<sub>2</sub>O<sub>3</sub> (9.14 Å<sup>3</sup>). The larger volume for rh-In<sub>2</sub>O<sub>3</sub> can be explained by the larger In ionic radius compared with that of Al. The main difference between both compounds is that octahedra are slightly more distorted in rh-In<sub>2</sub>O<sub>3</sub> than in rh-Al<sub>2</sub>O<sub>3</sub>, as evidenced by the slightly large difference in the bond distances between the two trigonal pyramids in both compounds: 2.1341 Å (In-O1) and 2.2599 Å (In-O2) for rh-In<sub>2</sub>O<sub>3</sub> and 1.8617 Å (Al-O1) and 1.9741 Å (Al-O2) for rh-Al<sub>2</sub>O<sub>3</sub>. The theoretical values of the In-O distances in rh-In<sub>2</sub>O<sub>3</sub> are in good agreement with our experimental values (2.1624 Å and 2.1836 Å) and experimental values previously reported (2.07 Å and 2.27 Å).<sup>21</sup> **Figure 5(a)** shows the experimental and theoretical pressure dependence of the  $A$ -O ( $A=Al, In$ ) relative bond distances in rh-In<sub>2</sub>O<sub>3</sub> and rh-Al<sub>2</sub>O<sub>3</sub> and **Table S5** (in the supplementary material) shows the linear fit of these theoretical data. As observed, the cation-anion bond lengths decrease with pressure at a higher rate in rh-In<sub>2</sub>O<sub>3</sub> than in rh-Al<sub>2</sub>O<sub>3</sub>. This different behaviour shows that rh-In<sub>2</sub>O<sub>3</sub> is more compressible (smaller bulk modulus) than rh-Al<sub>2</sub>O<sub>3</sub> in good agreement with our experimental volume data.

Another interesting issue of the calculations is the rather different decrease rate of the two cation-anion bond distances (In-O1 and In-O2) for the octahedron of rh-In<sub>2</sub>O<sub>3</sub> compared to those

of rh-Al<sub>2</sub>O<sub>3</sub> (Al-O1 and Al-O2), which decrease at a similar rate. This result indicates a quite different deformation of the AO<sub>6</sub> polyhedron in both compounds. In order to understand better the deformation in the octahedron with increasing pressure **Fig. 5(b)** displays the pressure dependence of the quadratic elongation ( $\lambda$ ) for rh-Al<sub>2</sub>O<sub>3</sub> and rh-In<sub>2</sub>O<sub>3</sub>, which gives a reliable indication of the distortion in the octahedron.<sup>81</sup> This parameter has been calculated by the average of the distortion in the bond-lengths implied in the octahedron, as described by equation (2),

$$\langle \lambda \rangle = \frac{1}{n} \sum_{i=1}^n \left( \frac{l_i}{l_0} \right)^2, \quad \text{Eq. (2)}$$

where  $l_i$  is the cation-anion bond length that forms the real polyhedron and  $l_0$  is the theoretical bond length in the most regular polyhedron. **Table S6** shows the linear and quadratic fit of the quadratic elongation for rh-Al<sub>2</sub>O<sub>3</sub> and rh-In<sub>2</sub>O<sub>3</sub>, respectively. As observed, the mean quadratic elongation of the polyhedron of rh-In<sub>2</sub>O<sub>3</sub> increases with pressure; i.e., the octahedron becomes more distorted as pressure increases. A similar behaviour has been found in hematite (rh-Fe<sub>2</sub>O<sub>3</sub>),<sup>72</sup> whereas the opposite is observed in rh-Al<sub>2</sub>O<sub>3</sub>, whose polyhedron becomes more regular with pressure. This trend could explain the high stability of rh-Al<sub>2</sub>O<sub>3</sub> under pressure. In fact, theoretical and experimental studies show the phase transition from rh-Al<sub>2</sub>O<sub>3</sub> to the Rh<sub>2</sub>O<sub>3</sub>-II-type (Pbcn) structure to occur above 96 GPa.<sup>81</sup> In contrast, rh-In<sub>2</sub>O<sub>3</sub> shows a much lower phase transition pressure (15 GPa) from rh-In<sub>2</sub>O<sub>3</sub> to o3-In<sub>2</sub>O<sub>3</sub> (Rh<sub>2</sub>O<sub>3</sub>-III-type or Pbca structure).

### C) RS measurements at high pressures

Selected Raman spectra of rh-In<sub>2</sub>O<sub>3</sub> at different pressures are reported on upstroke to 30.0 GPa (**Fig. 6(a)**) and downstroke to ambient pressure (**Fig. 6(b)**). From ambient pressure to 15.4 GPa, we can observe all seven Raman-active modes of rh-In<sub>2</sub>O<sub>3</sub> predicted by group theory. Above this pressure, we observed a decrease in the intensity of the Raman modes related to rh-

In<sub>2</sub>O<sub>3</sub>, being the lowest-frequency A<sub>1g</sub> mode, the last one in disappear above 26 GPa. Meanwhile, new peaks related to another phase (identified as o3-In<sub>2</sub>O<sub>3</sub>)<sup>42</sup> appear, being the dominant peak around 183 cm<sup>-1</sup> (see vertical arrow in **Fig. 6(a)**). Note that o3-In<sub>2</sub>O<sub>3</sub> is also characterized by two additional Raman modes around 142 and 239 cm<sup>-1</sup> at 15.4 GPa. This result is in good agreement with Raman results observed for this phase in Ref. 42. Thus, our RS measurements indicate that on upstroke rh-In<sub>2</sub>O<sub>3</sub> is stable up to 15 GPa and it coexists with a new phase (o3-In<sub>2</sub>O<sub>3</sub>) up to 26 GPa. In the downstroke process, the o3-In<sub>2</sub>O<sub>3</sub> phase is stable down to 8 GPa. Below that pressure, the sample transformed again in the metastable rh-In<sub>2</sub>O<sub>3</sub> phase (see **Fig. 6(b)**). Curiously, no coexistence is found between both phases on downstroke.

**Figure 7** shows the pressure dependence of the experimental and theoretical frequencies of the first-order Raman-active modes of rh-In<sub>2</sub>O<sub>3</sub>. Our frequencies at ambient pressure are in good agreement with previous reports<sup>25,35</sup> and with our *ab initio* calculations. Moreover, thanks to our *ab initio* calculations we have assigned the symmetry (A<sub>1g</sub> or E<sub>g</sub>) of the different observed Raman modes. As observed, all Raman-active mode frequencies increase with pressure in a monotonous way up to the maximum pressure attained in the experiment and a good agreement is found between the pressure dependence of experimental and theoretical frequencies of the first-order Raman-active modes.

**Table IV** summarizes the ambient pressure experimental and theoretical frequencies, pressure coefficients and the Grüneisen parameters of the Raman-active modes of rh-In<sub>2</sub>O<sub>3</sub> and rh-Al<sub>2</sub>O<sub>3</sub>. When comparing data of isostructural corundum-type In<sub>2</sub>O<sub>3</sub> and Al<sub>2</sub>O<sub>3</sub> in **Table IV** it can be observed that frequencies of the same modes are larger in Al<sub>2</sub>O<sub>3</sub> than in In<sub>2</sub>O<sub>3</sub> due to the smaller mass of Al than In. Moreover, the pressure coefficients of the two highest-frequency modes are much larger in rh-In<sub>2</sub>O<sub>3</sub> than in rh-Al<sub>2</sub>O<sub>3</sub>, thus showing a larger sensitivity to pressure

of Raman stretching modes in rh-In<sub>2</sub>O<sub>3</sub> than in rh-Al<sub>2</sub>O<sub>3</sub>. This result is in good agreement with the larger variation of In-O distances than of Al-O distances with increasing pressure already discussed. In fact, Grüneisen parameters are rather similar for the two highest-frequency modes in rh-In<sub>2</sub>O<sub>3</sub> and rh-Al<sub>2</sub>O<sub>3</sub>. Since the pressure coefficients of the stretching modes reflect the rate of decrease of interatomic cation-anion distances, the above result suggests that both compounds have similar sensitivity for stretching *A*-O forces. However, the Grüneisen parameters are smaller for low-frequency modes in rh-In<sub>2</sub>O<sub>3</sub> than in rh-Al<sub>2</sub>O<sub>3</sub>. Furthermore, both Grüneisen parameters for low- and high-frequency modes are similar in rh-Al<sub>2</sub>O<sub>3</sub> and quite different (up to a factor 1.7) in rh-In<sub>2</sub>O<sub>3</sub>. These results indicate a different sensitivity of both compounds for bending *A*-O forces and that both stretching and bending forces are more similar in rh-Al<sub>2</sub>O<sub>3</sub> than in rh-In<sub>2</sub>O<sub>3</sub>. All these results are in good agreement with the different distortion of the octahedral *AO*<sub>6</sub> units discussed in the previous section where an increase (decrease) of the regularity of octahedron in rh-Al<sub>2</sub>O<sub>3</sub> (rh-In<sub>2</sub>O<sub>3</sub>) has been observed. Now, the different distortion of the octahedron of the corundum structure can be understood as a consequence of the different behaviour of stretching and bending forces in this unit in both compounds.

Finally, we would like to stress that the higher sensitivity of rh-In<sub>2</sub>O<sub>3</sub> to compression than its isostructural compounds Al<sub>2</sub>O<sub>3</sub>, Ga<sub>2</sub>O<sub>3</sub>, and Cr<sub>2</sub>O<sub>3</sub> could be relevant for its use as pressure calibrant. The most usual method for pressure calibration in the laboratory relies on spectroscopic techniques. In particular, the pressure dependence of the photoluminescence lines R1 and R2 of ruby, assigned to internal transitions in the Cr<sup>3+</sup> cation, follows a well-known tendency.<sup>49,82</sup> However, the relatively small pressure coefficient of these lines leads to a considerable error in the determination of pressure in the low-pressure range. Therefore, the existence of compounds with structures more sensitive to pressure than ruby and with the

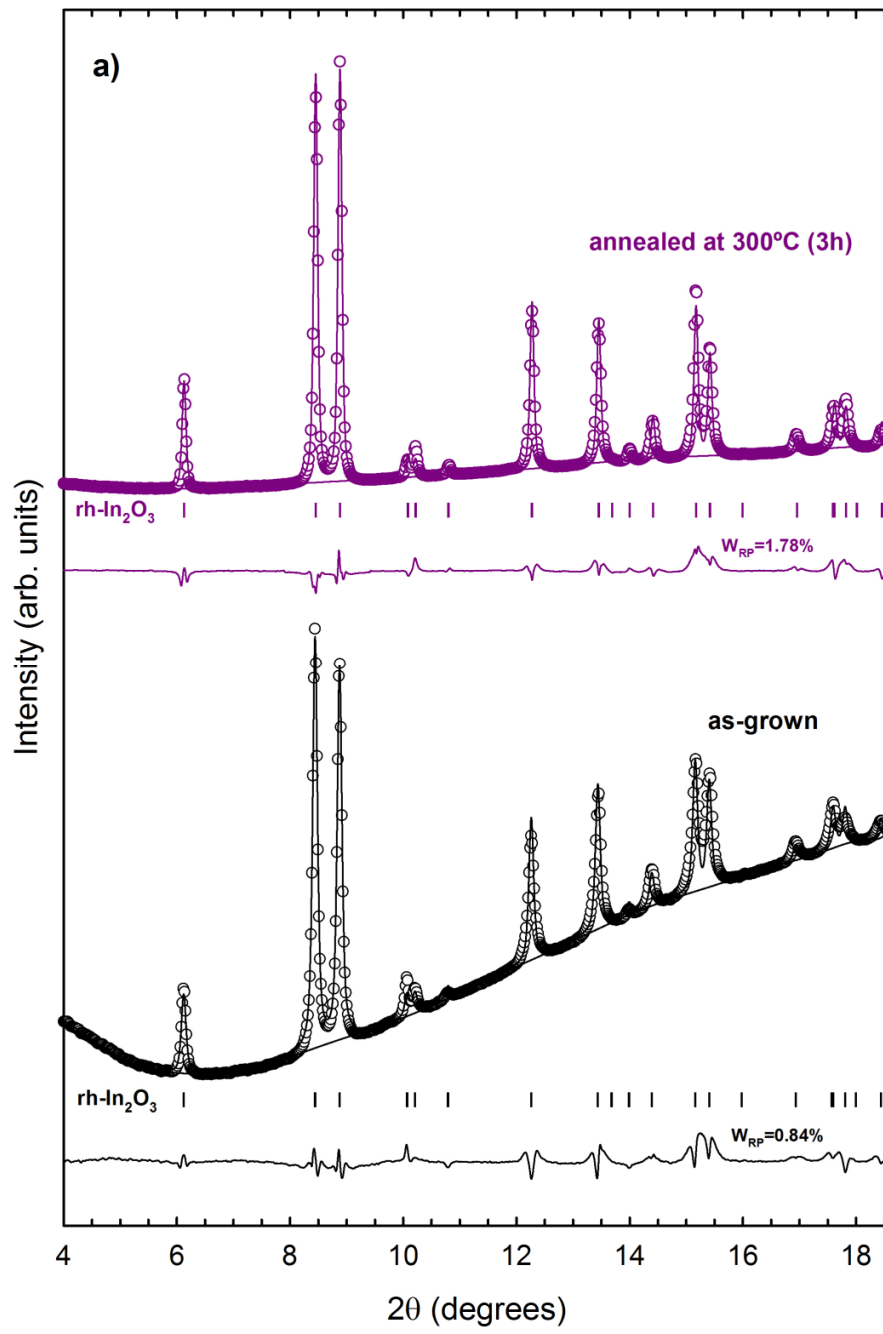
possibility to host  $\text{Cr}^{3+}$  cations opens a new path in the search for more accurate pressure sensors. In this context, the possibility to obtain metastable rh- $\text{In}_2\text{O}_3$  at ambient conditions (reported by many authors in the last years),<sup>36,41</sup> the stability of the rh- $\text{In}_2\text{O}_3$  up to 15 GPa at ambient temperature, and the low value of the bulk modulus of rh- $\text{In}_2\text{O}_3$  here reported suggest that  $\text{Cr}^{3+}$ -doped rh- $\text{In}_2\text{O}_3$  could be a possible candidate to substitute ruby at least below 15 GPa. It is expected that the higher sensitivity of the host material (rh- $\text{In}_2\text{O}_3$ ) would produce an increase in the pressure coefficient of the luminescence lines of  $\text{Cr}^{3+}$  with respect to ruby and consequently, a more accurate determination of pressure. However, for that purpose metastable corundum-type  $\text{Cr}^{3+}$ -doped  $\text{In}_2\text{O}_3$  must be prepared in an easy way as a single crystalline phase and its photoluminescence under pressure must be studied for different concentrations of  $\text{Cr}^{3+}$  doping.

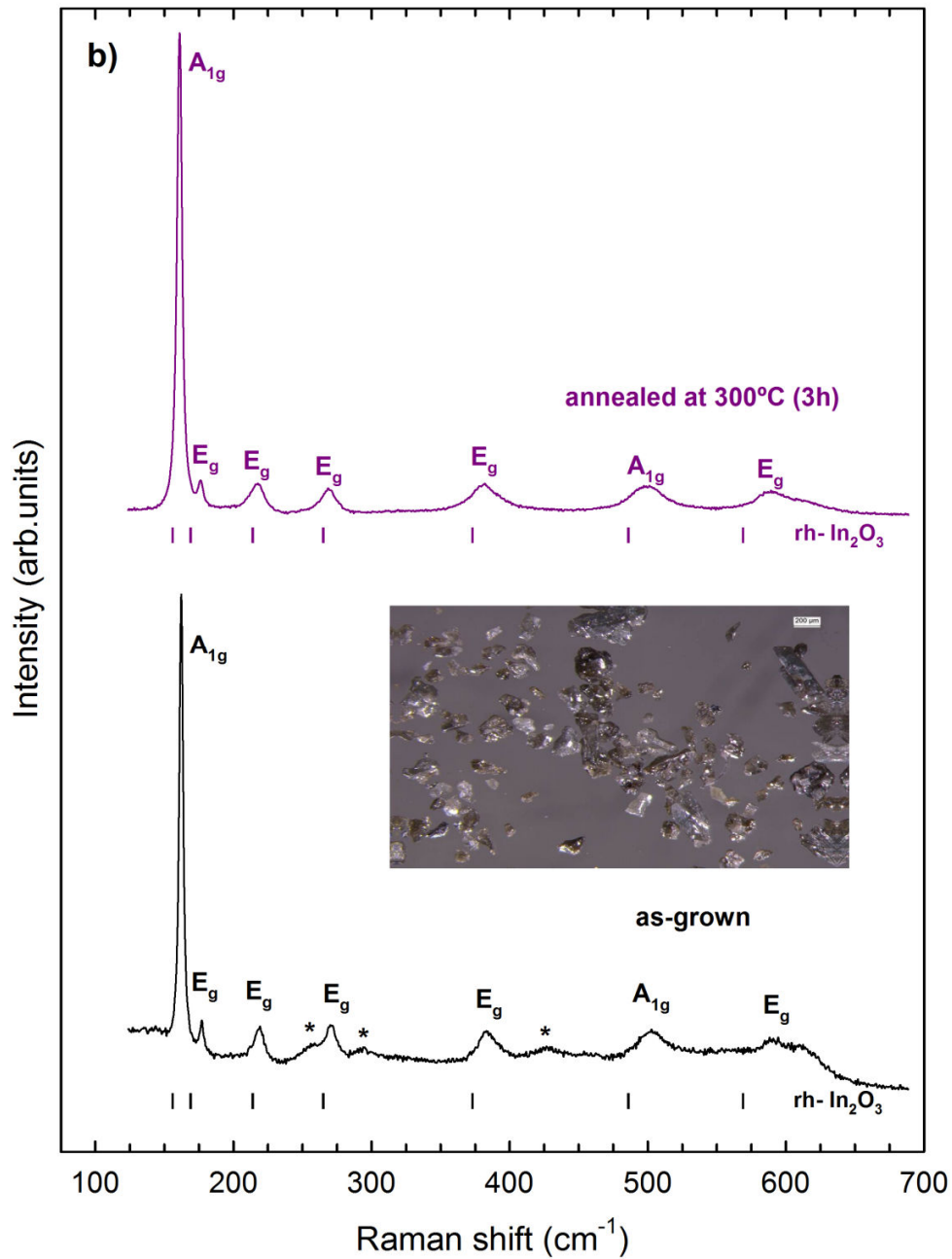
## CONCLUSIONS

We have synthesized rh- $\text{In}_2\text{O}_3$  at HP-HT in a multi-anvil cell and performed an experimental and theoretical study of their structural and vibrational properties under pressure. Thanks to XRD and RS measurements and *ab initio* calculations, we have performed a detailed and exhaustive comparison of the evolution of rh- $\text{In}_2\text{O}_3$  and rh- $\text{Al}_2\text{O}_3$  structures under pressure. XRD measurements in rh- $\text{In}_2\text{O}_3$  under pressure have allowed us to obtain an accurate experimental equation of state that is in good agreement with theoretical calculations. We have found a smaller bulk modulus for rh- $\text{In}_2\text{O}_3$  than for isomorphic rh- $\text{Al}_2\text{O}_3$ , rh- $\text{Ga}_2\text{O}_3$ , and rh- $\text{Cr}_2\text{O}_3$ . This result suggests the possibility to use  $\text{Cr}^{3+}$ -doped rh- $\text{In}_2\text{O}_3$  at ambient temperature as a more sensitive pressure sensor than ruby at least up to 15 GPa. The increase of the quadratic elongation parameter of rh- $\text{In}_2\text{O}_3$  with pressure suggests the presence of a mechanical instability of this structure at higher pressures. This result is in good agreement with the much lower

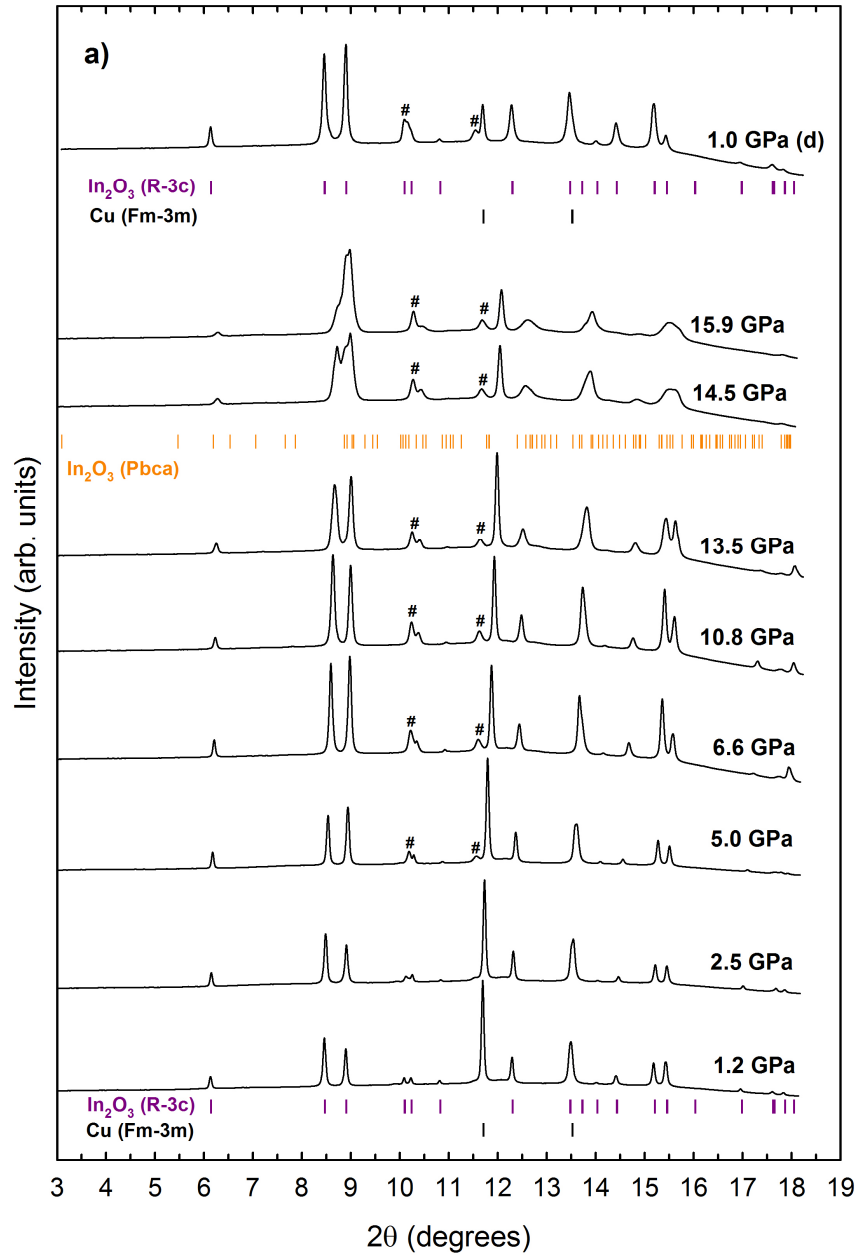
stability (phase transition pressure) of rh-In<sub>2</sub>O<sub>3</sub> than of rh-Al<sub>2</sub>O<sub>3</sub>. Our *ab initio* calculations have allowed us to assign the symmetry of the different observed first-order Raman active modes of rh-In<sub>2</sub>O<sub>3</sub>. RS measurements confirm the phase transition to o3-In<sub>2</sub>O<sub>3</sub> (Pbca-type) observed by angle-dispersive powder XRD above 14 GPa, as well as the behaviour of the octahedral unit and the cation-anion distances with increasing pressure as described by our theoretical calculations.

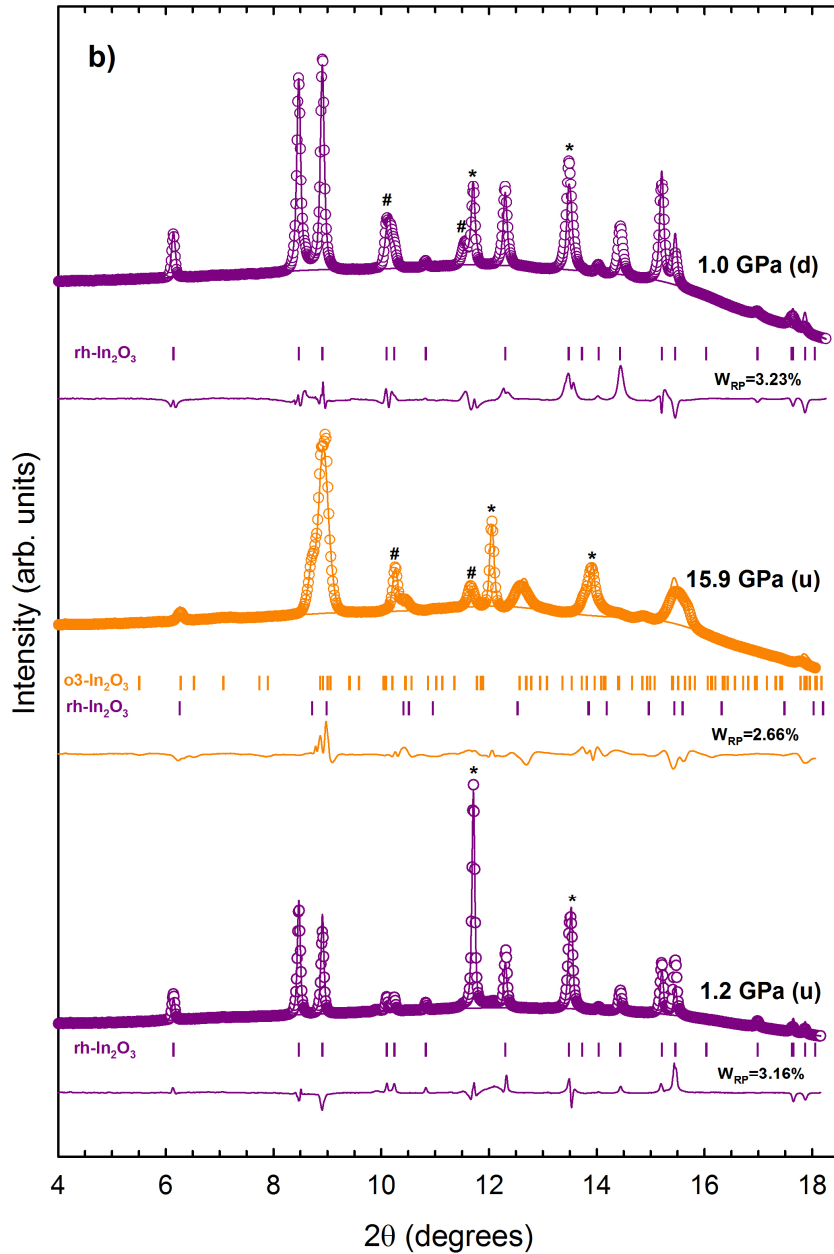
# FIGURES



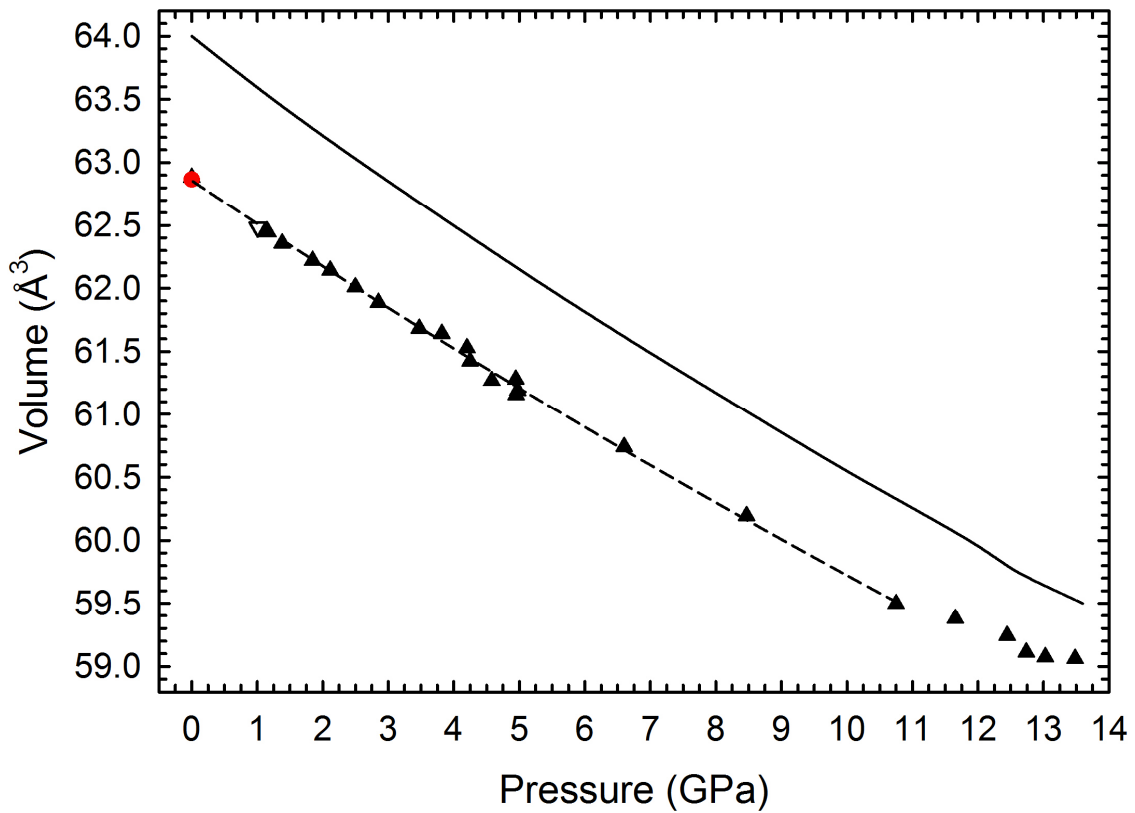


**Figure 1(a).** Angle-dispersive powder XRD pattern and **(b)** RS spectrum of rh-In<sub>2</sub>O<sub>3</sub> at ambient pressure. In both cases, the bottom pattern or spectrum corresponds to the as-grown sample while the upper one corresponds to the annealed sample. The seven first-order Raman-active modes theoretically predicted for the corundum phase are marked with vertical ticks at the bottom. Three modes not corresponding to first-order modes of rh-In<sub>2</sub>O<sub>3</sub> are observed in the as-grown sample (marked with and asterisk). Inset: Picture of the as-grown rh-In<sub>2</sub>O<sub>3</sub> micro-crystals.

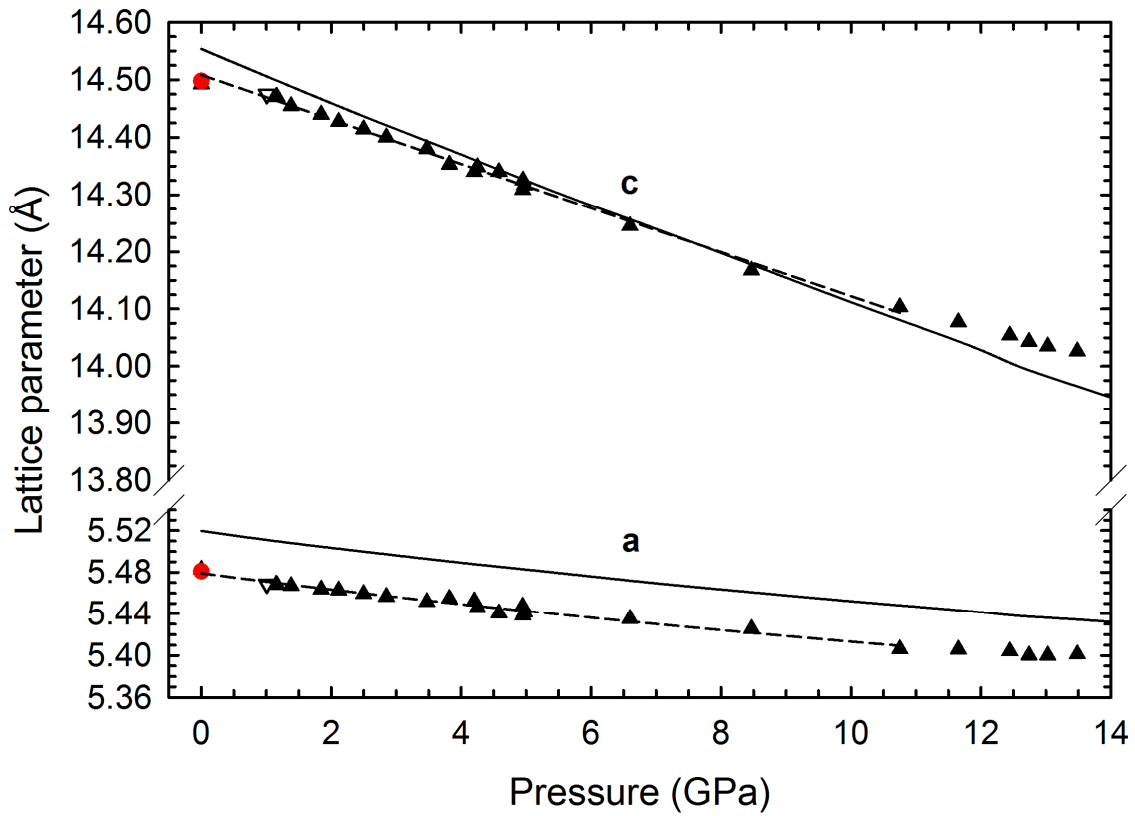




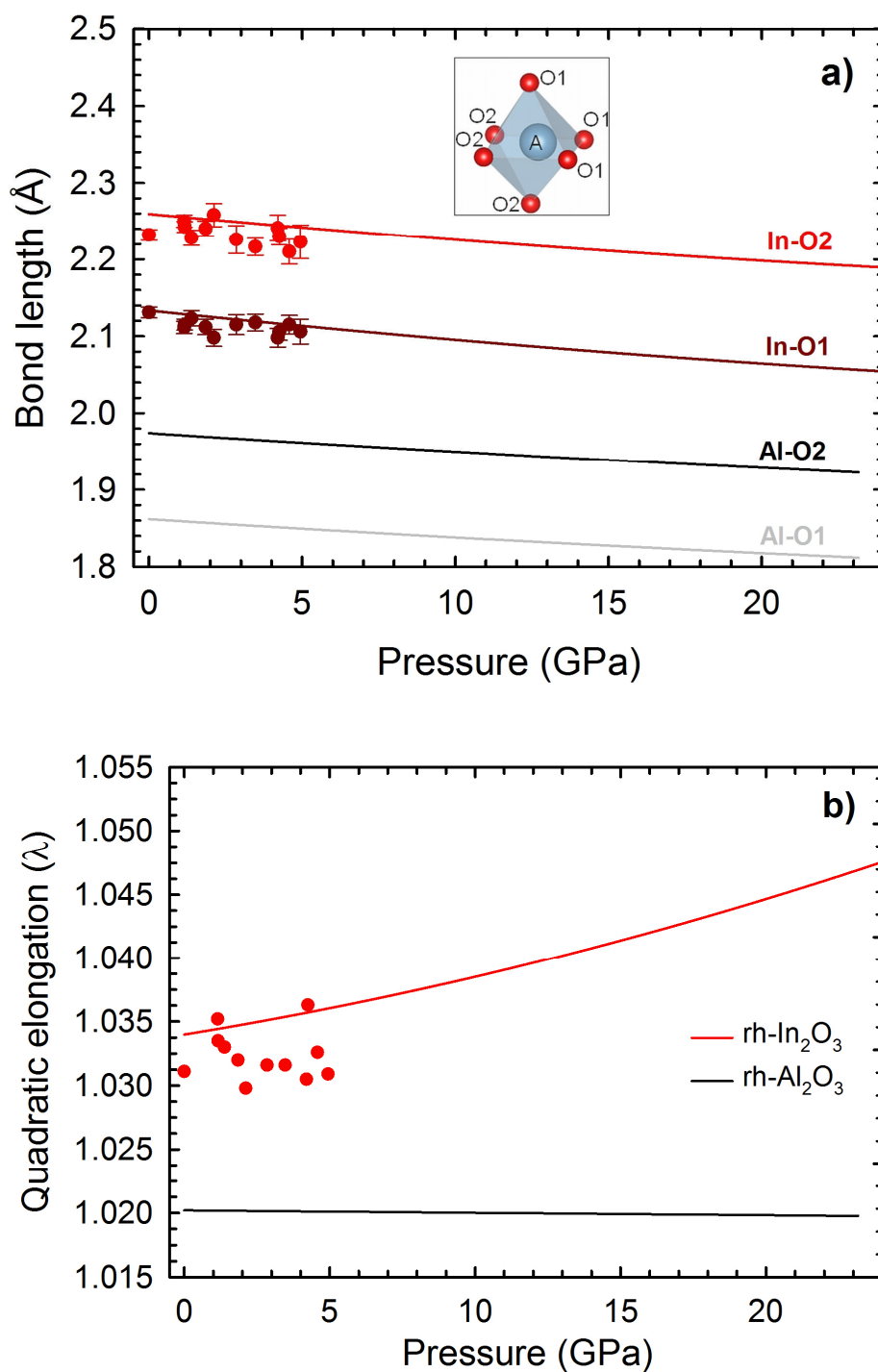
**Figure 2(a).** Selected X-ray diffraction patterns of  $\text{rh-In}_2\text{O}_3$  at several pressures up to 15.9 GPa. Diffractograms have been shifted vertically for clarity. Different Bragg reflections are assigned in the graph to their corresponding phase:  $\text{rh-In}_2\text{O}_3$  (R-3c) (|), cubic (Fm-3m) Cu (I) and  $\text{o3-In}_2\text{O}_3$  (Pbca) (I). Some impurities of hexagonal (P6<sub>3</sub>/mmc) Re are marked with (#). **(b)** Refinements of the experimental angle-dispersive XRD patterns on upstroke (u) at 1.2 GPa with the  $\text{rh-In}_2\text{O}_3$  and at 15.9 GPa with a mixture of  $\text{rh-In}_2\text{O}_3$  and  $\text{o3-In}_2\text{O}_3$  and on downstroke (d) at 1.0 GPa with the  $\text{rh-In}_2\text{O}_3$ . Residuals of the Rietveld refinements are plotted below the experimental (circles) and fitted (lines) X-ray diffraction profiles. Bragg reflections of Cu are assigned by (\*) and some impurities of hexagonal (P6<sub>3</sub>/mmc) Re are marked with (#).



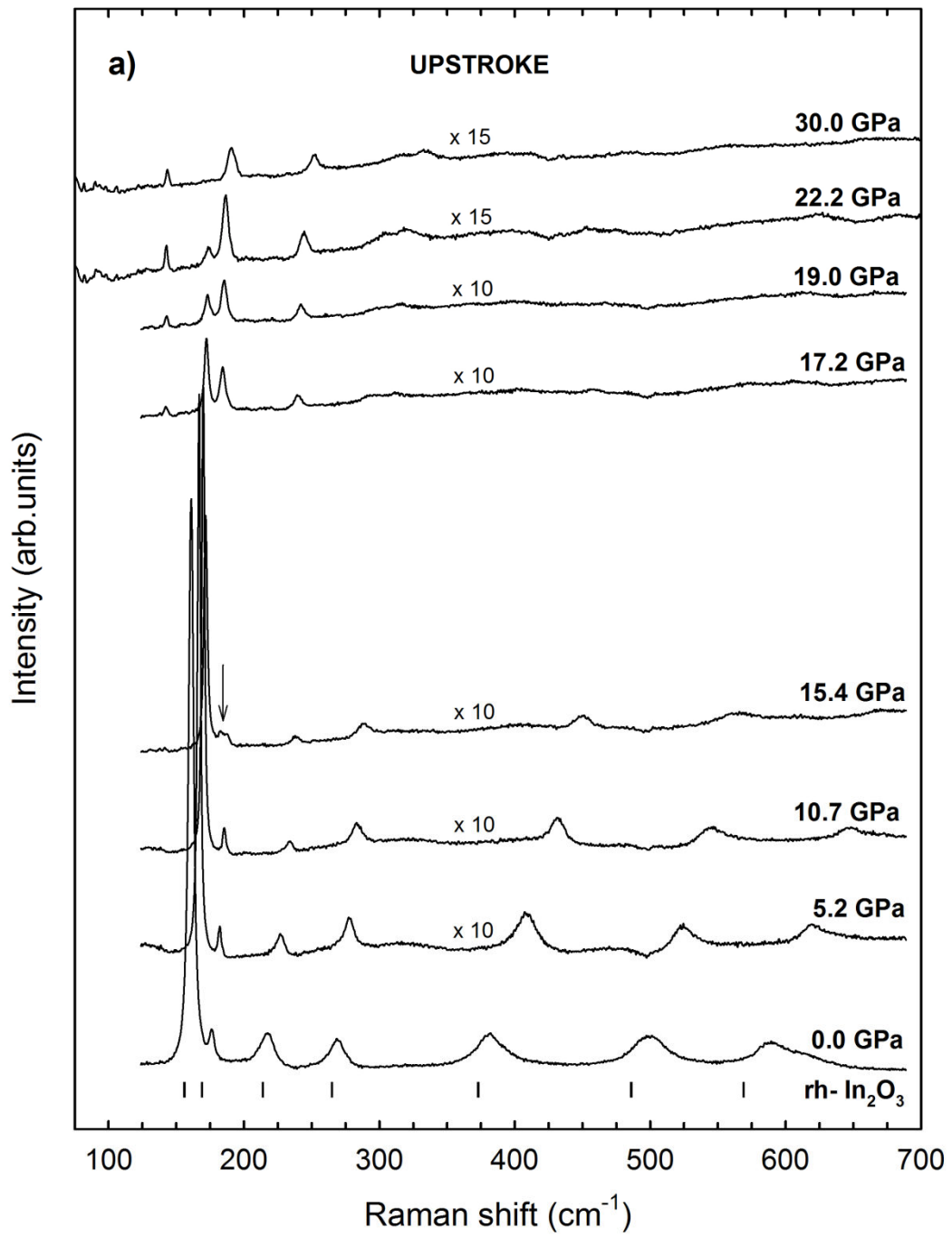
**Figure 3.** Pressure dependence of the unit-cell volume in rh-In<sub>2</sub>O<sub>3</sub>. Experimental data (triangles) during the upstroke (full) and downstroke (empty). The value at ambient pressure from Bekheet et al.<sup>41</sup> (red circle) is also shown for comparison. 3<sup>rd</sup> order Birch-Murnaghan EOS curves fitted to experimental data (dashed line) in the hydrostatic region of the PTM (below 11 GPa) and to theoretical data (solid line) are also shown.



**Figure 4.** Pressure dependence of the lattice parameters in rh-In<sub>2</sub>O<sub>3</sub>. Experimental data (triangles) during the upstroke (full) and downstroke (empty). The values at ambient pressure from Bekheet et al.<sup>41</sup> (red circle) are shown for comparison. Experimental data fit (dashed line) to the modified Murnaghan's equation in the hydrostatic region of the PTM and theoretical *ab initio* calculations (solid line) are also shown. Note that a different scale has been used for the vertical axes.



**Figure 5(a).** Pressure dependence of the experimental (circles) and theoretical (solid lines) cation-oxygen bond lengths of the  $AO_6$  polyhedron ( $A=Al, In$ ) in corundum-type  $A_2O_3$  sesquioxides. *Inset:* Representation of the  $AO_6$  polyhedron of the corundum phase in  $A_2O_3$  sesquioxides, where the cation is not located in the center of the polyhedron. **b)** Pressure dependence of the experimental (circles) and theoretical (solid lines) quadratic elongation of rh- $Al_2O_3$  and rh- $In_2O_3$ .



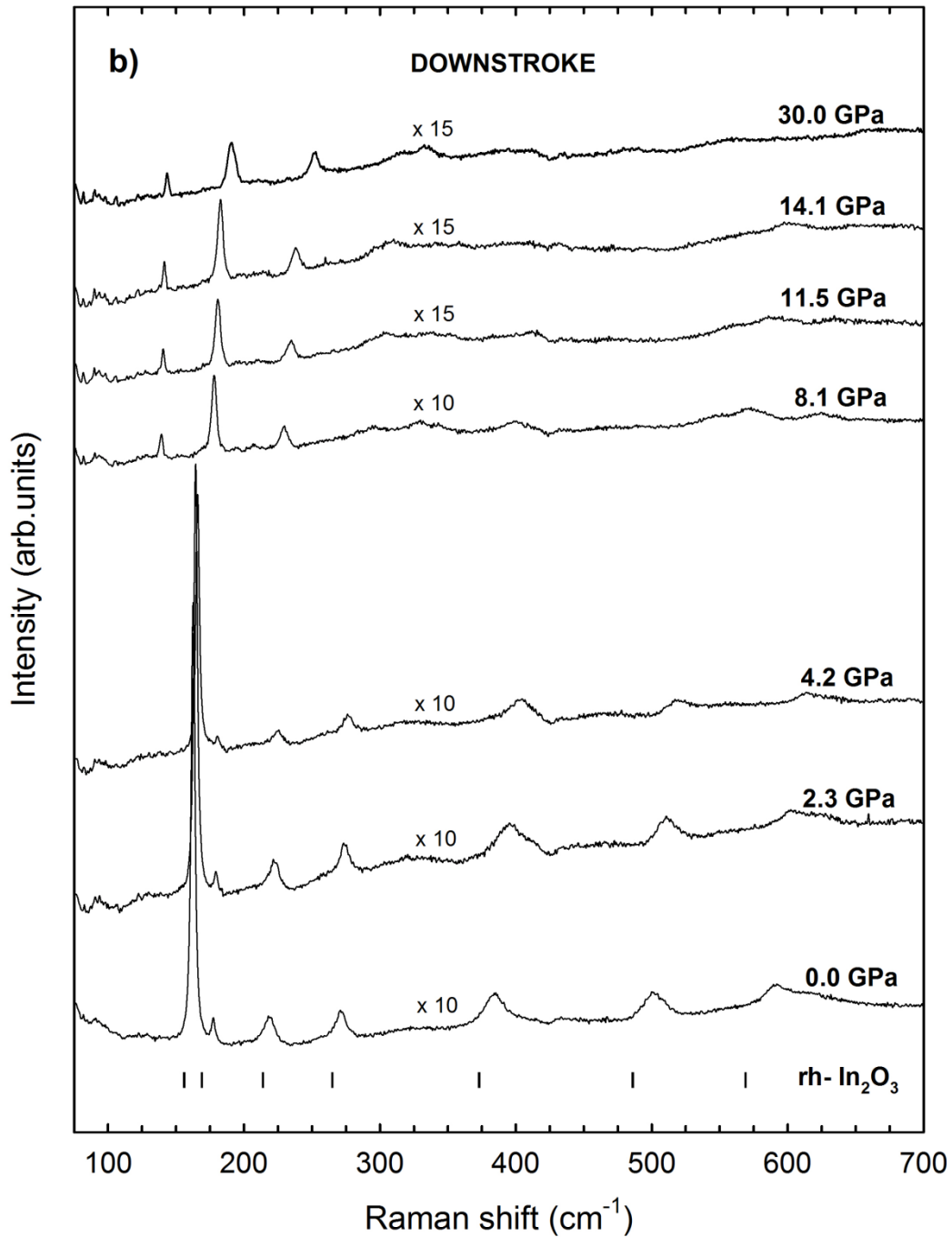


**Figure 6.** Selected RS spectra of rh-In<sub>2</sub>O<sub>3</sub> at different pressures on upstroke up to 30.0 GPa (a) and on downstroke down to ambient pressure (b). Ticks at the bottom of the Raman spectrum represent the *ab initio* calculations of the rh-In<sub>2</sub>O<sub>3</sub> Raman mode frequencies. RS spectra of o3-In<sub>2</sub>O<sub>3</sub> are taken in a longer wavenumber range than those of rh-In<sub>2</sub>O<sub>3</sub> in order to detect more first-order Raman-active modes in the former phase as predicted by *ab initio* calculations.

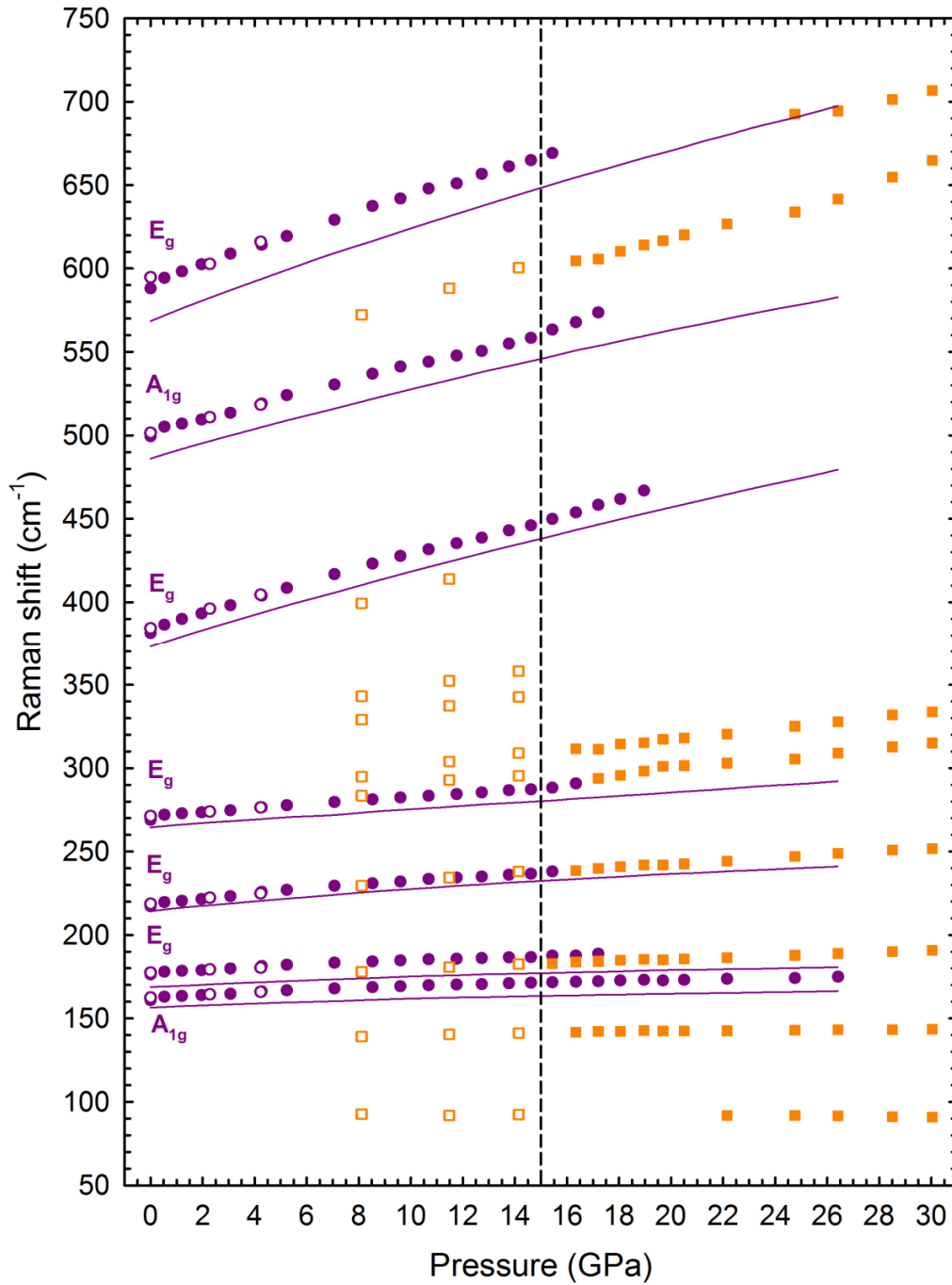


**Figure 7.** Pressure dependence of the Raman-mode frequencies of rh-In<sub>2</sub>O<sub>3</sub> (violet circles) and o3-In<sub>2</sub>O<sub>3</sub> (orange squares). Full (empty) symbols correspond to the upstroke (downstroke) process. The symmetry and the theoretical pressure dependence of Raman-active mode frequencies of rh-In<sub>2</sub>O<sub>3</sub> (solid lines) are also plotted.

## TABLES

**Table I.** Experimental (from Rietveld refinement) and theoretical values of the lattice parameters and atomic positions obtained for the rh-In<sub>2</sub>O<sub>3</sub> at ambient conditions. Values of previous works are given for comparison. The same atomic setting is employed to facilitate the comparison.

<i>a</i> (Å)	<i>c</i> (Å)	Method
5.483	14.493	Exp. <sup>a</sup>
5.487	14.510	Exp. <sup>b</sup>
5.490	14.520	Exp. <sup>c</sup>
5.481	14.498	Exp. <sup>d</sup>
5.519	14.554	Theo. <sup>a</sup>
5.493	14.424	Theo. <sup>e</sup>
5.479	14.415	Theo. <sup>f</sup>

<sup>a</sup> This work

<sup>b</sup> Refs. 20 and 22

<sup>c</sup> Ref. 21

<sup>d</sup> Ref. 41

<sup>e</sup> Ref. 42

<sup>f</sup> Ref. 43

rh-In <sub>2</sub> O <sub>3</sub>		Experimental			Theoretical		
Atom	Wyckoff site	x	y	z	x	y	z
In	12c	0	0	0.144 <sup>a</sup> 0.166 <sup>b</sup>	0	0	0.1426 <sup>a</sup> 0.1424 <sup>c</sup> 0.1423 <sup>d</sup>
O	18e	0.295 <sup>a</sup> 0.305 <sup>b</sup>	0	0.25	0.2958 <sup>a</sup> 0.2961 <sup>c</sup> 0.2954 <sup>d</sup>	0	0.25

<sup>a</sup> This work

<sup>b</sup> Ref. 21

<sup>c</sup> Ref. 44

<sup>d</sup> Ref. 45

**Table II.** Comparison of theoretical and experimental ambient pressure volume, bulk modulus, and its pressure derivative for the corundum-type structure (R-3c) of Al<sub>2</sub>O<sub>3</sub>, Ga<sub>2</sub>O<sub>3</sub>, and In<sub>2</sub>O<sub>3</sub>. Values for cubic-type (Ia-3) In<sub>2</sub>O<sub>3</sub> are also given for comparison. Last column indicates the EOS type used (BM2 = Birch-Murnaghan of 2<sup>nd</sup> order, BM3 = Birch-Murnaghan of 3<sup>rd</sup> order).

	Phase	V <sub>0</sub> (Å <sup>3</sup> )	B <sub>0</sub> (GPa)	B <sub>0</sub> '	Method	EOS type
Al <sub>2</sub> O <sub>3</sub>	R-3c	42.51	257 (6)	4	Exp. (XRD) <sup>a</sup>	BM2
	R-3c	42.8(4)	257 (1)	4	Theo. (GGA-PBEsol) <sup>b</sup>	BM2
	R-3c	42.41	240 (5)	3.97	Theo. (LDA) <sup>c</sup>	BM3
Ga <sub>2</sub> O <sub>3</sub>	R-3c	48.16 (4)	223 (2)	4	Exp. (XRD) <sup>d</sup>	BM2
	R-3c	47.24	243	4.0	Theo. (LDA) <sup>d</sup>	BM3
In <sub>2</sub> O <sub>3</sub>	R-3c	62.86 (3)	180 (7)	3.2 (1.2)	Exp. (XRD) <sup>b</sup>	BM3
	R-3c	62.87 (3)	176 (7)	4	Exp. (XRD) <sup>b</sup>	BM2
	R-3c		213 (8)	4.62	Exp. (XRD) <sup>e</sup>	BM3
	R-3c		215.2 (1.9)	4.74	Exp. (XRD) <sup>f</sup>	BM3
	R-3c	63.968 (12)	162.8 (2.0)	3.8 (3)	Theo. (GGA-PBEsol) <sup>b</sup>	BM3
	R-3c	63.993 (13)	161.3 (2.0)	4	Theo. (GGA-PBEsol) <sup>b</sup>	BM2
	R-3c	62.82	183.6	4.62	Theo. (LDA) <sup>g</sup>	BM3
	R-3c	63.25	182	3.0	Theo. (LDA) <sup>d</sup>	BM3
	R-3c	62.46	176	4.24	Theo. (LDA) <sup>h</sup>	BM3
	Ia-3	64.78	144 (8)	4	Exp. (XRD) <sup>d</sup>	BM2
	Ia-3	64.28 (13)	184 (10)	4	Exp. (XRD) <sup>i</sup>	BM2
Ia-3	65.72 (2)	169.4(1.2)	4	Theo. (GGA-PBEsol) <sup>i</sup>	BM2	

<sup>a</sup> Ref. 64

<sup>b</sup> This work

<sup>c</sup> Ref. 83

<sup>d</sup> Ref. 33

<sup>e</sup> Ref. 47

<sup>f</sup> Ref. 46

<sup>g</sup> Ref. 44

<sup>h</sup> Ref. 45

<sup>i</sup> Ref. 42

**Table III.** Theoretical and experimental lattice parameters, bulk modulus and pressure derivative of bulk modulus at ambient pressure in rh-In<sub>2</sub>O<sub>3</sub> obtained from a fit to modified Murnaghan's equation. The axial compressibilities  $\kappa_a$  and  $\kappa_c$  for the *a*- and *c*-axis are also included.

$a_0$ (Å)	$B_{0a}$ (GPa)	$B_{0a}'$	$\kappa_a$ ( $10^{-3}$ GPa <sup>-1</sup> )	$c_0$ (Å)	$B_{0c}$ (GPa)	$B_{0c}'$	$\kappa_c$ ( $10^{-3}$ GPa <sup>-1</sup> )	Method
5.479 (2)	220 (30)	11.8	1.5 (2)	14.511 (5)	121 (7)	0.48	2.75 (16)	Exp. (XRD)
5.5200 (3)	216 (3)	11.8 (4)	1.54 (2)	14.552 (1)	106.0 (0.9)	0.48 (11)	3.14 (3)	Theo. (GGA-PBEsol)

**Table IV.** Ambient-pressure experimental frequencies, pressure coefficients and Grüneisen parameters of the Raman active modes of rh-In<sub>2</sub>O<sub>3</sub> and rh-Al<sub>2</sub>O<sub>3</sub>.

Mode (Sym)	rh-In <sub>2</sub> O <sub>3</sub>								rh-Al <sub>2</sub> O <sub>3</sub>			
	<i>Ab initio</i> calculations				Experimental				Exp. <sup>c</sup>	Experimental <sup>d</sup>		
	$\omega_0$ (cm <sup>-1</sup> )	$\frac{\partial \omega}{\partial P}$ $\left(\frac{cm^{-1}}{GPa}\right)$	$\frac{\partial^2 \omega}{\partial P^2}$ $\left(\frac{cm^{-1}}{GPa^2}\right)$	$\gamma^a$	$\omega_0$ (cm <sup>-1</sup> )	$\frac{\partial \omega}{\partial P}$ $\left(\frac{cm^{-1}}{GPa}\right)$	$\frac{\partial^2 \omega}{\partial P^2}$ $\left(\frac{cm^{-1}}{GPa^2}\right)$	$\gamma^b$	$\omega_0$ (cm <sup>-1</sup> )	$\omega_0$ (cm <sup>-1</sup> )	$\frac{\partial \omega}{\partial P}$ $\left(\frac{cm^{-1}}{GPa}\right)$	$\gamma$
<b>A<sub>1g</sub></b>	156(1)	0.65 (3)	-0.012 (2)	0.66	162.3 (2)	0.85 (4)	-0.015 (1)	0.92	164	418.5	1.70	1.15
<b>E<sub>g</sub></b>	169(1)	0.73 (3)	-0.010 (2)	0.68	177.1 (2)	1.01 (6)	-0.022 (3)	1.00		378.4	1.34	0.99
<b>E<sub>g</sub></b>	214(1)	1.54 (3)	-0.023 (2)	1.14	218.1 (3)	1.85 (8)	-0.039 (5)	1.49	221.8	430.6	2.79	1.73
<b>E<sub>g</sub></b>	265(1)	1.11 (6)	-0.005 (5)	0.66	270.7 (4)	1.33 (13)	-0.011 (7)	0.86	273	448.7 <sup>e</sup>	1.66 <sup>e</sup>	1.05 <sup>e</sup>
									309			
<b>E<sub>g</sub></b>	373(2)	4.91 (5)	-0.040 (4)	2.08	383.8 (6)	4.69 (16)	-0.022 (8)	2.15	385	576.4	2.76	1.28
<b>A<sub>1g</sub></b>	486(2)	4.46 (6)	-0.033 (4)	1.45	501.9 (9)	3.92 (25)	0.005 (14)	1.37	504.5	645.2	3.48	1.49
<b>E<sub>g</sub></b>	569(2)	6.14 (5)	-0.059 (4)	1.70	590.3 (6)	5.95 (18)	-0.058 (12)	1.77	596	750.6	4.22	1.52

<sup>a</sup> Obtained with theoretical B<sub>0</sub>= 158 GPa.

<sup>b</sup> Obtained with experimental B<sub>0</sub>= 176 GPa.

<sup>c</sup> Ref. 25

<sup>d</sup> Ref. 84

<sup>e</sup> Ref. 85

## **AUTHOR INFORMATION**

### **Corresponding Author**

\*(J.A. Sans) E-mail: juasant2@upv.es. Telephone: (+34) 963877000 ext(75287).

### **Author Contributions**

The manuscript was written through contributions of all authors. All authors have given approval to the final version of the manuscript.

### **Notes**

The authors declare no competing financial interest.

## **ACKNOWLEDGMENT**

This work is supported by the Spanish MICINN projects MAT2013-46649-C4-1/2/3-P and CSD2007-00045 and by the Generalitat Valenciana under projects GV06/151 and ACOMP/2014/243. A.M. and P.R-H acknowledge computing time provided by Red Española de Supercomputación (RES) and MALTA-Cluster. B.G-D and J.A.S. acknowledge financial support through the FPI program and Juan de la Cierva fellowship. S.V.O. acknowledges the financial support of the Deutsche Forschungsgemeinschaft (DFG) under project OV-110/1-2.

## REFERENCES

- 1 Mizoguchi H.; Woodward P.M. Electronic Structure Studies of Main Group Oxides Possessing Edge-Sharing Octahedra: Implications for the Design of Transparent Conducting Oxides. *Chem. Mater.* **2004**, 16, 5233-5248.
- 2 Granqvist C. G. Transparent Conductive Electrodes for Electrochromic Devices: A Review. *Appl. Phys. A.* **1993**, 57, 19.
- 3 Ellmer, K. Past Achievements and Future Challenges in the Development of Optically Transparent Electrodes. *Nat. Photonics* **2012**, 6, 809-817.
- 4 Walsh A.; Da Silva J.L.F.; Wei S.H. Multi-Component Transparent Conducting Oxides: Progress in Materials Modelling. *J. Phys.: Condens. Matter* **2011**, 23, 334210
- 5 Hoel C.A.; Mason T.O.; Gaillard J.F.; Poepelmeier K.R. Transparent Conducting Oxides in the ZnO-In<sub>2</sub>O<sub>3</sub>-SnO<sub>2</sub> System. *Chem. Mater.* **2010**, 22, 3569-3579.
- 6 Breeze A.J.; Schlesinger Z.; Carter S.A.; Brock P.J. Charge Transport in TiO<sub>2</sub>/MEH-PPV Polymer Photovoltaics. *Phys. Rev. B* **2001**, 64, 125205.
- 7 Tahar R.B.H.; Ban T.; Ohya Y.; Takahashi Y. Tin Doped Indium Oxide Thin Films: Electrical Properties. *J. Appl. Phys.* **1998**, 83, 2631-2645.
- 8 Kaspar, T. C.; Droubay, T.; Jaffe, J. E. ZnO/Sn:In<sub>2</sub>O<sub>3</sub> and ZnO/CdTe Band Offsets for Extremely Thin Absorber Photovoltaics. *Appl. Phys. Lett.* **2011**, 99, 263504.
- 9 Tang C.W; Vanslyke S.A. Organic Electroluminescent Diodes. *Appl. Phys. Lett.* **1987**, 51, 913-915.
- 10 Tang L.-M.; Wang L.-L; Wang D.; Liu J.-Z; Chen K.-Q. Donor-Donor Binding in In<sub>2</sub>O<sub>3</sub>: Engineering Shallow Donor Levels. *J. Appl. Phys.* **2010**, 107, 083704.

- 11 Steele B.C.H.; Golden S.J. Variable Transmission Electrochromic Windows Utilizing Tin-Doped Indium Oxide Counterelectrodes. *Appl. Phys. Lett.* **1991**, 59, 2357.
- 12 Lee B.H.; Kim I.G.; Cho S.W.; Lee S.H. Effect of Process Parameters on the Characteristics of Indium Tin Oxide Thin Film for Flat Panel Display Application. *Thin Solid Films* **1997**, 302, 25-30.
- 13 Hsu S.F.; Lee C.C.; Hwang S.W.; Chen C.H. Highly Efficient Top-Emitting White Organic Electroluminescent Devices. *Appl. Phys. Lett.* 2005, **86**, 253508.
- 14 Himmerlich M.; Wang Ch.Y.; Cimalla V.; Ambacher O.; Krischok S. Surface Properties of Stoichiometric and Defect-Rich Indium Oxide Films Grown by MOCVD. *J. Appl. Phys.* 2012, **111**, 093704.
- 15 Lai X.Y.; Wang D.; Han N.; Du J.; Li J.; Xing C.J.; Chen Y.F.; Li X.T. Ordered Arrays of Bead-Chain-Like  $\text{In}_2\text{O}_3$  Nanorods and Their Enhanced Sensing Performance for Formaldehyde. *Chem. Mater.* **2010**, 22, 3033-3042.
- 16 Rauf I.A. Low Resistivity and High Mobility Tin-Doped Indium Oxide Films. *Mater. Lett.* **1993**, 18, 123-127.
- 17 Palmer G. B.; Poepelmeier K. R.; Mason T. O. Conductivity and Transparency of ZnO/SnO<sub>2</sub>-Cosubstituted  $\text{In}_2\text{O}_3$ . *Chem. Mater.* **1997**, 9, 3121-3126.
- 18 Hoel C.A.; Amores J.M.G.; Moran E.; Alario-Franco M.A.; Gaillard J.F.; Poepelmeier K.R. High-Pressure Synthesis and Local Structure of Corundum-Type  $\text{In}_{2-2x}\text{Zn}_x\text{Sn}_x\text{O}_3$  ( $x \leq 0.7$ ). *J. Am. Chem. Soc.* **2010**, 132, 16479-16487.

- 19 Marezio M. Refinement of Crystal Structure of  $\text{In}_2\text{O}_3$  at 2 Wavelengths. *Acta Crystallogr.* **1966**, 20, 723-728.
- 20 Shannon R.D. New High Pressure Phases Having Corundum Structure. *Solid State Commun.* **1966**, 4, 629-630.
- 21 Christen A.N.; Broch N.C. Hydrothermal Investigation of Systems  $\text{In}_2\text{O}_3\text{-H}_2\text{O-Na}_2\text{O}$  and  $\text{In}_2\text{O}_3\text{-D}_2\text{O-Na}_2\text{O}$ . Crystal Structure of Rhombohedral  $\text{In}_2\text{O}_3$  and of  $\text{In}(\text{OH})_3$ . *Act. Chem. Scand.* **1967**, 21, 1046-1056.
- 22 Prewitt C.T.; Shannon R.D.; Rogers D.B.; Sleight A.W. C Rare Earth Oxide-Corundum Transition and Crystal Chemistry of Oxides Having Corundum Structure. *Inorg. Chem.* **1969**, 8, 1985-1993.
- 23 Atou T.; Kusaba K.; Fukuoka K.; Kikuchi M.; Syono Y. Shock-Induced Phase-Transition of  $\text{Sc}_2\text{O}_3$ -Type,  $\text{Y}_2\text{O}_3$ -Type,  $\text{Sm}_2\text{O}_3$ -Type,  $\text{Gd}_2\text{O}_3$ -Type,  $\text{In}_2\text{O}_3$ -Type Compounds. *J. Solid State Chem.* **1990**, 89, 378-384.
- 24 Gurlo A.; Barsan N.; Weimar U.; Ivanovskaya M.; Taurino A.; Siciliano P. Polycrystalline Well-Shaped Blocks of Indium Oxide Obtained by the Sol-Gel Method and their Gas-Sensing Properties. *Chem. Mater.* **2003**, 15, 4377-4383.
- 25 Yu D.B.; Yu S.H.; Zhang S.Y.; Zuo J.; Wang D.B.; Qian Y.T. Metastable Hexagonal  $\text{In}_2\text{O}_3$  Nanofibers Templated from  $\text{InOOH}$  Nanofibers under Ambient Pressure. *Adv. Funct. Mater.* **2003**, 13, 497-501.
- 26 Seo W.S.; Jo H.H.; Lee K.; Park J.T. Preparation and Optical Properties of Highly Crystalline, Colloidal, and Size-Controlled Indium Oxide Nanoparticles. *Adv. Mater.* **2003**, 15, 795-797.

- 27 Epifani M.; Siciliano P.; Gurlo A.; Barsan N., Weimar U. Ambient Pressure Synthesis of Corundum-Type  $\text{In}_2\text{O}_3$ . *J. Am. Chem. Soc.* **2004**, 126, 4078-4079.
- 28 Yu D.B.; Wang D.B.; Qian Y.T. Synthesis of Metastable Hexagonal  $\text{In}_2\text{O}_3$  Nanocrystals by a Precursor-Dehydration Route under Ambient Pressure. *J. Solid State Chem.* **2004**, 177, 1230-1234.
- 29 Sorescu M.; Diamandescu L.; Tarabasanu-Mihaila D.; Teodorescu V.S. Nanocrystalline Rhombohedral  $\text{In}_2\text{O}_3$  Synthesized by Hydrothermal and Postannealing Pathways. *J. Mat. Sci.* **2004**, 39, 675-677.
- 30 Lee C.H.; Kim M.; Kim T.; Kim A.; Paek J.; Lee J.W.; Choi S.Y.; Kim K.; Park J.B.; Lee K. Ambient Pressure Syntheses of Size-Controlled Corundum-Type  $\text{In}_2\text{O}_3$  Nanocubes. *J. Am. Chem. Soc.* **2006**, 128, 9326-9327.
- 31 Chen C.L.; Chen D.R.; Jiao X.L.; Wang C.Q. Ultrathin Corundum-Type  $\text{In}_2\text{O}_3$  Nanotubes Derived from Orthorhombic  $\text{InOOH}$ : Synthesis and Formation Mechanism. *Chem. Commun.* **2006**, 44, 4632-4634.
- 32 Xu J.Q.; Chen Y.P.; Pan Q.Y.; Xiang Q.; Chen Z.X.; Dong X.W. A New Route for Preparing Corundum-Type  $\text{In}_2\text{O}_3$  Nanorods Used as Gas-Sensing Materials. *Nanotech.* **2007**, 18, 115615.
- 33 Yusa H.; Tsuchiya T.; Sata N., Ohishi Y.  $\text{Rh}_2\text{O}_3(\text{II})$ -Type Structures in  $\text{Ga}_2\text{O}_3$  and  $\text{In}_2\text{O}_3$  Under High Pressure: Experiment and Theory. *Phys. Rev. B* **2008**, 77, 064107.
- 34 Yusa H.; Tsuchiya T.; Tsuchiya J.; Sata N.; Ohishi Y. Alpha- $\text{Gd}_2\text{S}_3$ -Type Structure in  $\text{In}_2\text{O}_3$ : Experiments and Theoretical Confirmation of a High-Pressure Polymorph in Sesquioxide. *Phys. Rev. B* **2008**, 78, 092107.

- 35 Wang C.Y.; Dai Y.; Pezoldt J.; Lu B.; Kups T.; Cimalla V.; Ambacher O. Phase Stabilization and Phonon Properties of Single Crystalline Rhombohedral Indium Oxide. *Cryst. Growth Des.* **2008**, 8, 1257-1260.
- 36 Saitoh H.; Utsumi W.; Aoki K. Solid-Phase Grain Growth of  $\text{In}_2\text{O}_3$  at High Pressures and Temperatures. *J. Cryst. Growth* **2008**, 310, 2295-2297.
- 37 Gurlo A.; Dzivenko D.; Kroll P.; Riedel R. High-Pressure High-Temperature Synthesis of  $\text{Rh}_2\text{O}_3$ -II-Type  $\text{In}_2\text{O}_3$  Polymorph. *Phys. Stat. Sol. RRL* **2008**, 2, 269-271.
- 38 Gurlo A.; Kroll P.; Riedel R. Metastability of Corundum-Type  $\text{In}_2\text{O}_3$ . *Chem-Eur. J.* **2008**, 14, 3306-3310.
- 39 Gurlo A. Structural Stability of High-Pressure Polymorphs in  $\text{In}_2\text{O}_3$  Nanocrystals: Evidence of Stress-Induced Transition? *Angew. Chem. Int. Ed.* **2010**, 49, 5610-5612.
- 40 Bekheet M.F.; Schwarz M.R.; Lauterbach S.; Kleebe H.J.; Kroll P.; Riedel R.; Gurlo A. Orthorhombic  $\text{In}_2\text{O}_3$ : A Metastable Polymorph of Indium Sesquioxide. *Angew. Chem. Int. Ed.* **2013**, 52, 6531-6535.
- 41 Bekheet M.F.; Schwarz M.R.; Lauterbach S.; Kleebe H.J.; Kroll P.; Stewart A.; Kolb U.; Riedel R.; Gurlo A. In Situ High Pressure High Temperature Experiments in Multi-Anvil Assemblies with Bixbyite-Type  $\text{In}_2\text{O}_3$  and Synthesis of Corundum-Type and Orthorhombic  $\text{In}_2\text{O}_3$  Polymorphs. *High Press. Res.* **2013**, 33, 697-711.
- 42 García-Domene B.; Sans J.A.; Gomis O.; Manjón F.J.; Ortiz H.M.; Errandonea D.; Santamaría-Pérez D.; Martínez-García D.; Vilaplana R.; Pereira A.L.J. et al. Pbc-Type  $\text{In}_2\text{O}_3$ : The High-Pressure Post-Corundum Phase at Room Temperature. *J. Phys. Chem C* **2014**, 118, 20545-20552.

- 43 Beales T.P.; Goodman C.H.L.; Scarrott K. A New High-Pressure Calibrant: Beta- $\text{Ga}_2\text{O}_3\text{:Cr}$ . *Solid State Commun.* **1990**, 73, 1-3.
- 44 Karazhanov S. Zh.; Ravindran P.; Vajeeston P.; Ulyashin A.; Finstad T.G.; Fjellvag H. Phase Stability, Electronic Structure, and Optical Properties of Indium Oxide Polytypes. *Phys. Rev. B* **2007**, 76, 075129.
- 45 Fuchs F.; Bechstedt F. Indium-Oxide Polymorphs from First Principles: Quasiparticle Electronic States. *Phys. Rev. B* **2008**, 77, 155107.
- 46 Qi J.; Liu J.F.; He Y.; Chen W.; Wang C. Compression Behavior and Phase Transition of Cubic  $\text{In}_2\text{O}_3$  Nanocrystals. *J. Appl. Phys.* **2011**, 109, 063520.
- 47 Liu D.; Lei W.W.; Zou B.; Yu S.D.; Hao J.; Wang K.; Liu B.B.; Cui Q.L.; Zou G.T. High-Pressure X-Ray Diffraction and Raman Spectra Study of Indium Oxide. *J. Appl. Phys.* **2008**, 104, 083506.
- 48 Dewaele A.; Loubeyre P.; Mezouar M. Equations of State of Six Metals above 94 GPa. *Phys. Rev. B* **2004**, 70, 094112.
- 49 Syassen K. Ruby under Pressure. *High Press. Res.* **2008**, 28, 75-126.
- 50 Fauth F.; Peral I.; Popescu C.; Knapp M. The New Material Science Powder Diffraction Beamline at ALBA Synchrotron. *Powder. Diffr.* **2013**, 28, S360-S370.
- 51 Hammersley A.P.; Svensson S.O.; Hanfland M.; Fitch A.N.; Häusermann D. Two-Dimensional Detector Software: From Real Detector to Idealised Image or Two-Theta Scan. *High Press. Res.* **1996**, 14, 235-248.
- 52 Kraus W.; Nolze G. Powder Cell - A Program for the Representation and Manipulation of Crystal Structures and Calculation of the Resulting X-Ray Powder Patterns. *J. Appl. Crystallogr.* **1996**, 29, 301-303.

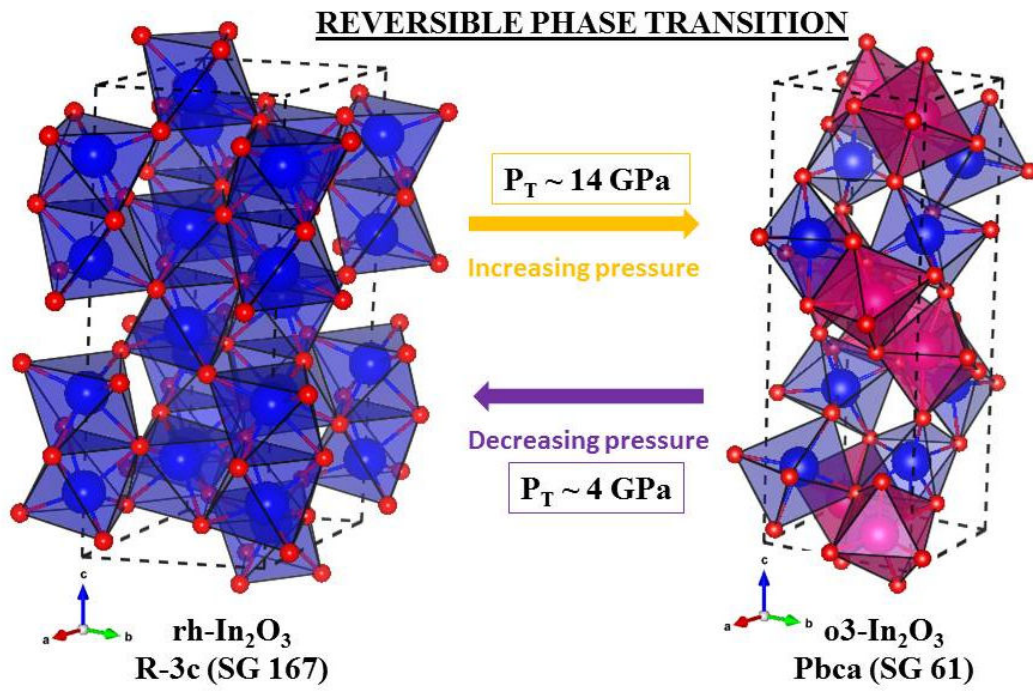
- 53 Toby B.H. EXPGUI, A Graphical User Interface for GSAS. *J. Appl. Crystallogr.* **2001**, 34, 210-213.
- 54 Hohenberg P.; Kohn W. Inhomogeneous Electron Gas. *Phys. Rev. B* **1964**, 136, 864-871.
- 55 Kresse G.; Hafner J. Ab Initio Molecular Dynamics for Liquid Metals. *Phys. Rev. B* **1993**, 47, 558-561.
- 56 Blöchl P.E. Projector Augmented-Wave Method. *Phys. Rev. B* **1994**, 50, 17953-17979.
- 57 Perdew J.P.; Ruzsinszky A.; Csonka G.I.; Vydrov O.A.; Suseria G.E.; Constantin L.A.; Zhou X.; Burke K. Restoring the Density-Gradient Expansion for Exchange in Solids and Surfaces. *Phys. Rev. Lett.* **2008**, 100, 136406.
- 58 Parlinski K. Computer Code PHONON. See: <http://wolf.ifj.edu.pl/phonon>.
- 59 García-Domene B.; Ortiz H.M.; Gomis O.; Sans J.A.; Manjón F.J.; Muñoz A.; Rodríguez-Hernández P.; Achary S.N.; Errandonea D.; Martínez-García D.; et al. High-Pressure Lattice Dynamical Study of Bulk and Nanocrystalline In<sub>2</sub>O<sub>3</sub>. *J. Appl. Phys.* **2012**, 112, 123511.
- 60 Boultif A.; Louer D. Powder Pattern Indexing with the Dichotomy Method. *J. Appl. Cryst.* **2004**, 37, 724-731.
- 61 Robinson K.; Gibbs G.V.; Ribbe P.H. Quadratic Elongation: A Quantitative Measure of Distortion in Coordination Polyhedra. *Science* **1971**, 172, 567-570.
- 62 Klotz S.; Chervin J-C.; Munsch P.; Le Marchand G. Hydrostatic Limits of 11 Pressure Transmitting Media. *J. Phys. D: Appl. Phys.* **2009**, 42, 075413.
- 63 Errandonea D.; Ruiz-Fuertes J.; Sans J.A.; Santamaría-Perez D.; Gomis O.; Gomez A.; Sapina F. Compressibility and Structural Stability of Ultra-Incompressible Bimetallic Interstitial Carbides and Nitrides. *Phys. Rev. B* **2012**, 85, 144103.

- 64 Murnaghan F.D. The Compressibility of Media under Extreme Pressures. *Proc. Nat. Acad. Sci.* **1944**, 30, 244-247.
- 65 Birch F. Finite Elastic Strain of Cubic Crystals. *Phys. Rev.* **1947**, 71, 809-824.
- 66 Finger L.W.; Hazen R.M. Crystal Structure and Compression of Ruby to 46 kbar. *J. Appl. Phys.* **1978**, 49, 5823-5826.
- 67 Machon D.; McMillan P.F.; Xu B.; Dong J. High-Pressure Study of the Beta-to-Alpha Transition in Ga<sub>2</sub>O<sub>3</sub>. *Phys. Rev. B* **2006**, 73, 094125.
- 68 Nishio-Hamame D.; Katagiri M.; Niwa K.; Sano-Furukawa A.; Okada T.; Yagi T. A New High-Pressure Polymorph of Ti<sub>2</sub>O<sub>3</sub>: Implication for High-Pressure Phase Transition in Sesquioxides. *High Press. Res.* **2009**, 29, 379-388.
- 69 Ovsyannikov S.V.; Wu X.; Karkin A.E.; Shchennikov V.V.; Manthilake G.M. Pressure-Temperature Phase Diagram of Ti<sub>2</sub>O<sub>3</sub> and Physical Properties in the Golden Th<sub>2</sub>S<sub>3</sub>-Type Phase. *Phys. Rev. B* **2012**, 86, 024106.
- 70 Sato Y.; Akimoto S. Hydrostatic Compression of 4 Corundum Type Compounds: Alpha-Al<sub>2</sub>O<sub>3</sub>, V<sub>2</sub>O<sub>3</sub>, Cr<sub>2</sub>O<sub>3</sub>, and Alpha-Fe<sub>2</sub>O<sub>3</sub>. *J. Appl. Phys.* **1979**, 50, 5285-5291.
- 71 Dera P.; Lavina B.; Meng Y.; Prakapenka V.B. Structural and Electronic Evolution of Cr<sub>2</sub>O<sub>3</sub> on Compression to 55 GPa. *J. Solid State Chem.* **2011**, 184, 3040-3049.
- 72 Rozenberg G.K.; Dubrovinsky L.S.; Pasternak M.P.; Naaman O.; Le Bihan T.; Ahuja R. High-Pressure Structural Studies of Hematite Fe<sub>2</sub>O<sub>3</sub>. *Phys. Rev. B* **2002**, 65, 064112.
- 73 Ovsyannikov S.V.; Trots D.M.; Kurnosov A.V.; Morgenroth W.; Liermann H.P.; Dubrovinsky L. Anomalous Compression and New High-Pressure Phases of Vanadium Sesquioxide, V<sub>2</sub>O<sub>3</sub>. *J. Phys.: Condens. Matter* **2013**, 25, 385401.

- 74 Zhang Q.; Wu X.; Qin S. Pressure-Induced Phase Transition of  $V_2O_3$ . *Chin. Phys. Lett.* **2012**, 29, 106101.
- 75 McWhan D.B.; Remeika J.P. Metal-Insulator Transition in  $(V_{1-x}Cr_x)_2O_3$ . *Phys. Rev. B* **1970**, 2, 3734-3750.
- 76 Finger L.W.; Hazen R.M. Crystal Structure and Isothermal Compression of  $Fe_2O_3$ ,  $Cr_2O_3$ , and  $V_2O_3$  to 50 kbars. *J. Appl. Phys.* **1980**, 51, 5362-5367.
- 77 Hart H.V.; Drickamer H.G. Effect of High Pressure on the Lattice Parameters of  $Al_2O_3$ . *J. Chem. Phys.* **1965**, 43, 2265-2266.
- 78 Richet P.; Xu J.A.; Mao H.K. Quasi-Hydrostatic Compression of Ruby to 500 Kbar. *Phys. Chem. Miner.* **1988**, 16, 207-211.
- 79 Damour H.; Schiferl D.; Denner W.; Schulz H.; Holzapfel W.B. High-Pressure Single-Crystal Structure Determinations for Ruby up to 90 Kbar Using an Automatic Diffractometer. *J. Appl. Phys.* **1978**, 49, 4411-4416.
- 80 Jephcoat A.P.; Hemley R.J.; Mao H.K. X-Ray-Diffraction of Ruby ( $Al_2O_3:Cr^{3+}$ ) to 175 GPa. *Physica B* **1988**, 150, 115-121.
- 81 Marton F.C.; Cohen R.E. Prediction of a High-Pressure Phase-Transition in  $Al_2O_3$ . *Am. Miner.* **1994**, 79, 789-792.
- 82 Mao H.K.; Xu J.; Bell P.M. Calibration of the Ruby Pressure Gauge to 800 Kbar under Quasi-Hydrostatic Conditions. *J. Geophys. Res.* **1986**, 91, 4673-4676.
- 83 Tsuchiya J.; Tsuchiya T.; Wentzcovitch R.M. Transition from the  $Rh_2O_3(II)$ -to- $CaIrO_3$  Structure and the High-Pressure-Temperature Phase Diagram of Alumina. *Phys. Rev. B* **2005**, 72, 020103.

- 84 Xu J.A.; Huang E.; Lin J.F.; Xu L.Y. Raman Study at High Pressure and the Thermodynamic Properties of Corundum: Application of Kieffer's Model. *Am. Mineral.* **1995**, 80, 1157-1165.
- 85 Watson G.H.; Daniels W.B.; Wang C.S. Measurements of Raman Intensities and Pressure-Dependence of Phonon Frequencies in Sapphire. *J. Appl. Phys.* **1981**, 52, 956-958.

TOC ABSTRACT GRAPHICS



Supplementary material of  
**Synthesis and High-Pressure Study of Corundum-Type  $\text{In}_2\text{O}_3$**

*B. García-Domene,<sup>1</sup> J.A. Sans,<sup>2,\*</sup> F. J. Manjón,<sup>2</sup> Sergey V. Ovsyannikov,<sup>3</sup> L.S. Dubrovinsky,<sup>3</sup> D. Martínez-García,<sup>1</sup> O. Gomis,<sup>4</sup> D. Errandonea,<sup>1</sup> H. Moutaabbid,<sup>5</sup> Y. Le Godec,<sup>5</sup> H.M. Ortiz,<sup>2,6</sup> A. Muñoz,<sup>7</sup> P. Rodríguez-Hernández,<sup>7</sup> and C. Popescu<sup>8</sup>*

<sup>1</sup> Departamento de Física Aplicada-ICMUV, MALTA Consolider Team, Universidad de Valencia, Edificio de Investigación, C/Dr. Moliner 50, Burjassot, 46100 Valencia, Spain

<sup>2</sup> Instituto de Diseño para la Fabricación y Producción Automatizada, MALTA Consolider Team-Universitat Politècnica de València, 46022 València, Spain

<sup>3</sup> Bayerisches Geoinstitut, Universität Bayreuth, Universitätsstrasse 30, D-95447, Bayreuth, Germany

<sup>4</sup> Centro de Tecnologías Físicas: Acústica, Materiales y Astrofísica, MALTA Consolider Team, Universitat Politècnica de València, 46022 València, Spain

<sup>5</sup> Institut de Minéralogie, de Physique des Matériaux, et de Cosmochimie (IMPMC)-Sorbonne Universités, UPMC Université Paris 06, UMR CNRS 7590, Muséum National d'Histoire Naturelle, IRD UMR 206, 4 Place Jussieu, F-75005 Paris, France

<sup>6</sup> CINVESTAV-Departamento de Nanociencia y Nanotecnología, Unidad Querétaro, 76230 Querétaro, México

<sup>7</sup> Departamento de Física, Instituto de Materiales y Nanotecnología, MALTA Consolider Team, Universidad de La Laguna, 38205 Tenerife, Spain

<sup>8</sup> CELLS-ALBA Synchrotron, E-08290 Cerdanyola, Barcelona, Spain

**Figure S1.** Typical CCD images of angle-dispersive powder X-ray diffraction for the annealed sample (300 °C) at ambient pressure (a) and 10.8 GPa (b).

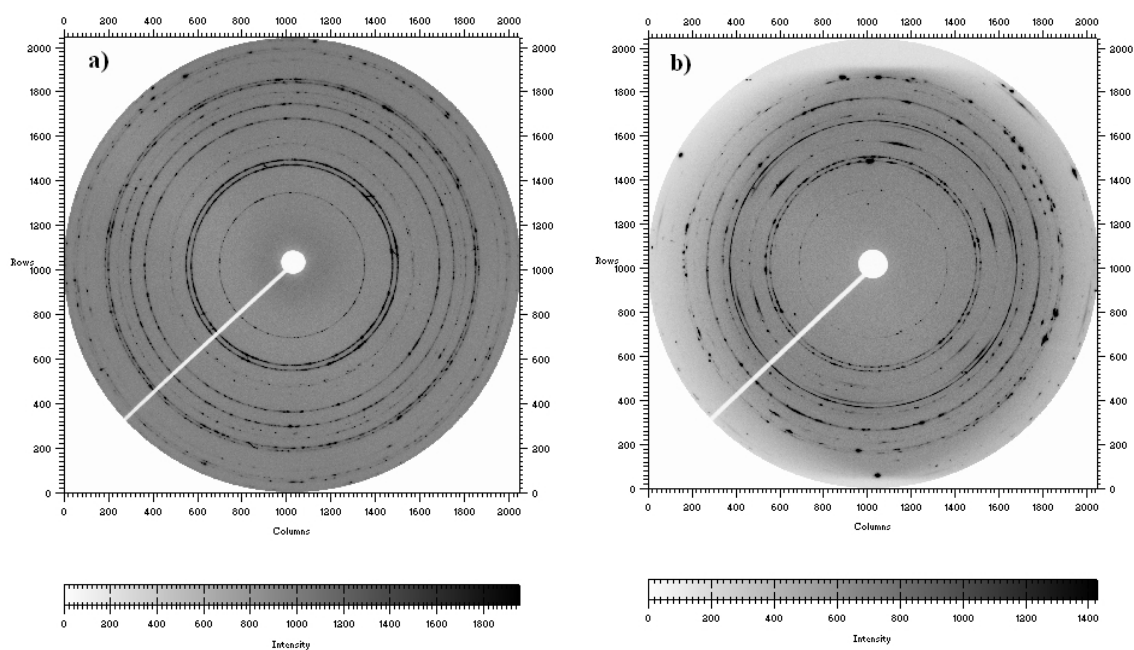


**Figure S2.** Experimental (circles) and theoretical (solid lines) pressure dependence of the (X, 0, 0.25) and (0, 0, Z) atomic positions of 18e (O) and 12c (In) Wyckoff positions, respectively in corundum-type  $\text{In}_2\text{O}_3$ . Experimental results have been obtained from Rietveld refinements of XRD data.

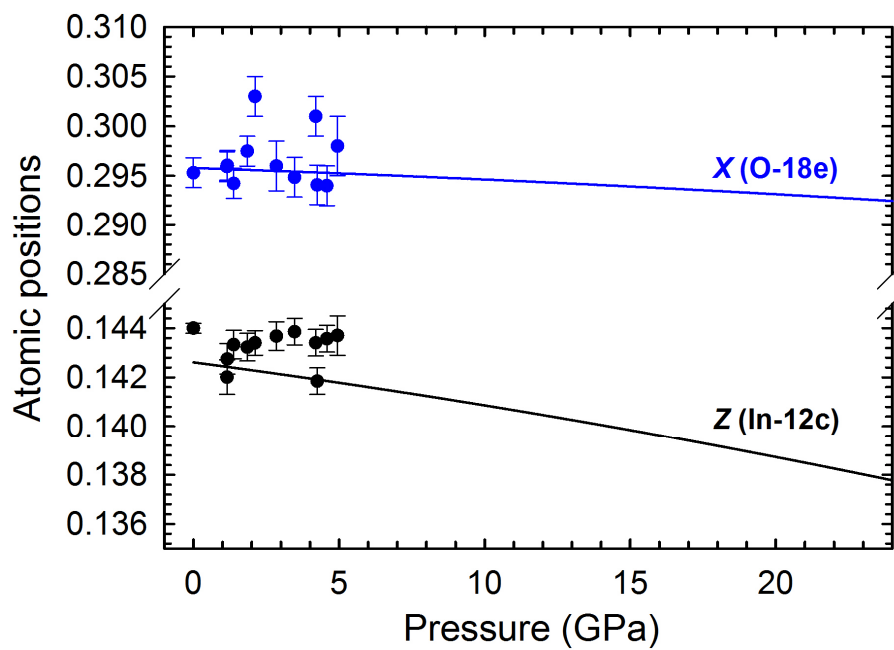


**Table S1.** Experimental and theoretical values of lattice parameters and atomic positions of rh-In<sub>2</sub>O<sub>3</sub>.

rh-In <sub>2</sub> O <sub>3</sub>	P (GPa)	a (Å)	c (Å)	Atom	Wyckoff site	x	y	z
Experimental	1.2	5.4637 (3)	14.4399 (12)	In	12c	0	0	0.1427
				O	18e	0.2980	0	0.25
Theoretical	1.1	5.5092	14.4950	In	12c	0	0	0.1424
				O	18e	0.2954	0	0.25

**Table S2.** Experimental and theoretical values of lattice parameters and atomic positions of rh-In<sub>2</sub>O<sub>3</sub> and o3-In<sub>2</sub>O<sub>3</sub>.

rh-In <sub>2</sub> O <sub>3</sub>	P (GPa)	a (Å)	c (Å)	Atom	Wyckoff site	x	y	z
Experimental	15.9	5.421 (4)	13.906 (10)	In	12c	0	0	0.1495
				O	18e	0.2937	0	0.25
Theoretical	16.3	5.4214	13.8484	In	12c	0	0	0.1395
				O	18e	0.2937	0	0.25

o3-In <sub>2</sub> O <sub>3</sub>	P (GPa)	a (Å)	b (Å)	c (Å)	Atom	Wyckoff site	x	y	z
Experimental	15.9	5.378 (3)	5.494 (3)	14.516 (8)	In1	8c	0.0003	0.7840	0.4310
					In2	8c	0.9675	0.7732	0.1789
					O1	8c	0.3591	0.8682	0.2012
					O2	8c	0.2062	0.5109	0.3757
					O3	8c	0.1455	0.6525	0.0531
Theoretical	16.1	5.4105	5.5251	15.5220	In1	8c	0.0003	0.7840	0.4310
					In2	8c	0.9974	0.7305	0.1830
					O1	8c	0.3591	0.8682	0.2012
					O2	8c	0.2062	0.5109	0.3757
					O3	8c	0.1455	0.6525	0.0531

**Table S3.** Experimental (during downstroke) and theoretical values of the lattice parameters and atomic positions of rh-In<sub>2</sub>O<sub>3</sub>.

R-3c	P (GPa)	a (Å)	c (Å)	Atom	Wyckoff site	x	y	z
Experimental	1.0	5.4687 (3)	14.4751 (15)	In	12c	0	0	0.1436
				O	18e	0.2816	0	0.25
Theoretical	1.1	5.5092	14.4950	In	12c	0	0	0.1424
				O	18e	0.2954	0	0.25

**Table S4.** Theoretical pressure dependence of the (x, 0, 0.25) and (0, 0, z) atomic positions for the 18e (O) and 12c (In) Wyckoff positions, from a quadratic fit to  $x=x_0+\gamma P+\delta P^2$  and  $z=z_0+\gamma P+\delta P^2$ , respectively.

	$x_0$ or $z_0$	$\gamma$ ( $10^{-4}$ GPa <sup>-1</sup> )	$\delta$ ( $10^{-6}$ GPa <sup>-2</sup> )
x (O – 18e)	0.29579 (3)	-0.99 (4)	-1.64 (13)
z (In – 12c)	0.14261 (2)	-1.56 (2)	-1.87 (5)

**Table S5.** Theoretical cation-oxygen bond lengths in the  $AO_6$  polyhedron ( $A=Al, In$ ) at ambient pressure and its pressure coefficient in corundum-type  $A_2O_3$  sesquioxides from a linear fit to  $l(P)=l_0+dl/dP \cdot P$ .

	$l_0$ (Å)	$dl/dP$ (Å/GPa)
<b>Al – O1</b>	1.8604 (4)	-0.00216 (3)
<b>Al – O2</b>	1.9728 (4)	-0.00223 (3)
<b>In – O1</b>	2.129 (1)	-0.00316 (6)
<b>In – O2</b>	2.2555 (9)	-0.00280 (5)

**Table S6.** Theoretical quadratic elongation ( $\lambda$ ) and its pressure derivatives for rh- $Al_2O_3$  (after a linear fit to  $\lambda=\lambda_0+\alpha P$ ) and rh- $In_2O_3$  (after a quadratic fit to  $\lambda=\lambda_0+\alpha P+\beta P^2$ ).

	$\lambda_0$	$\alpha$ ( $10^{-5} \text{ GPa}^{-1}$ )	$\beta$ ( $10^{-6} \text{ GPa}^{-2}$ )
<b>rh-<math>Al_2O_3</math></b>	1.0202	-1.875 (2)	
<b>rh-<math>In_2O_3</math></b>	1.03398 (5)	37.2 (7)	8.1 (3)